J. Fluid Mech. (1991), *vol.* 228, *pp.* 487–511
Printed in Great Britain

Influence of wrinkled premixed-flame dynamics on large-scale, low-intensity turbulent flow

By R. C. ALDREDGE AND F. A. WILLIAMS
Department of Applied Mechanics and Engineering Sciences, University of California, San Diego, La Jolla, CA 92093-0310, USA

(Received 16 January 1990 and in revised form 11 December 1990)

Premixed turbulent flame propagation is analysed under the assumptions of stationarity and transverse homogeneity by expansions for small values of the ratio of the turbulence intensity to the laminar burning velocity. For large Zel'dovich numbers, the effects of diffusive–thermal phenomena within the flame, gas expansion, buoyancy and Lewis and Prandtl numbers different from unity are taken into account under the constraint that turbulence scales are large compared with the laminar flame thickness. A general formulation is given, involving solutions through Fourier decompositions. Parametric results for turbulent burning velocities are obtained, and the evolution of components of turbulent kinetic energies through the flame is calculated. It is shown how buoyancy counteracts the tendency for gas expansion to increase transverse components of the turbulent kinetic energy, pressure fluctuations and vorticity generation across the wrinkled flame. Strong readjustments in components of the turbulent kinetic energy are shown to occur in the downstream hydrodynamic zone. It is established that, with the effects of the hydrodynamic zones fully taken into account, the flame can induce anisotropy in initially isotropic turbulence such that the final velocity fluctuations exhibit higher intensities in the longitudinal mode than in transverse modes, while the enhanced vorticity fluctuations are entirely transverse.

1. Introduction

Although there are many applications in which it is important to know effects of premixed flames on turbulent flows, the calculation of these effects from first principles is notoriously difficult. One of many lines of approach to the problem has been through a perturbation analysis in a small parameter ϵ representing the ratio of a laminar flame thickness d to a turbulence scale l (Clavin & Williams 1979; 1982; Searby & Clavin 1986). Although limited by the range of validity of the expansions employed, this type of approach has the advantage of yielding predictions free from arbitrary modelling hypotheses. The present study adopts the formulation of this earlier work (Clavin & Williams 1982; Searby & Clavin 1986), but with the relative turbulence intensity δ, the ratio of a root-mean-square velocity fluctuation to the laminar burning velocity, treated as an additional independent parameter, and addresses the evaluation of properties of turbulent flames that have not been fully explored in the earlier investigations.

General characteristics of the flame structure obtained as an expansion in ϵ are illustrated in figure 1. The laminar flame, of thickness d, appears as a moving, wrinkled discontinuity in the analysis. The equation of motion of the discontinuity and the jump conditions across it depend on the structure of the laminar flame and

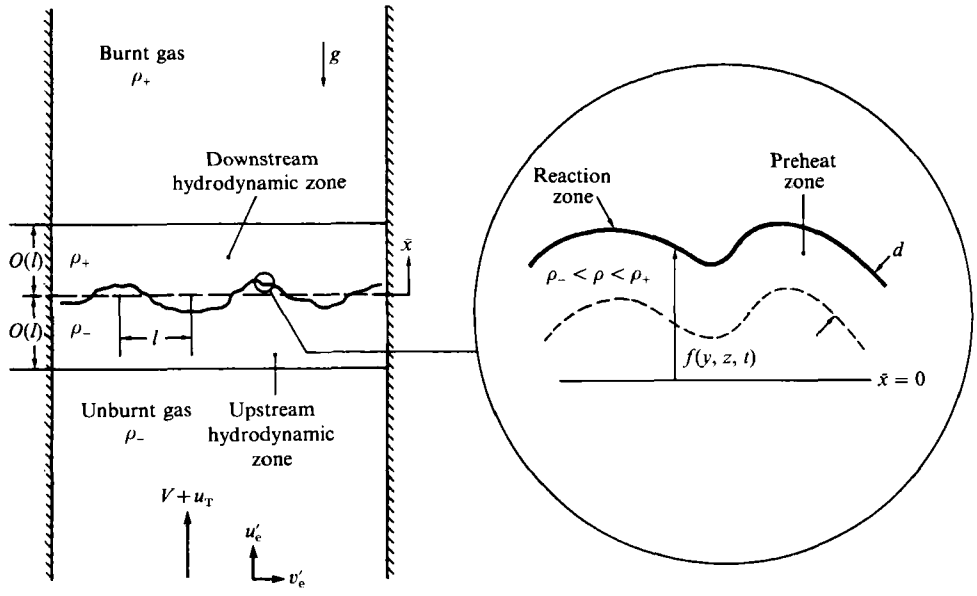

FIGURE 1. The arrangement of zones for the wrinkled laminar flame.

can be characterized in general for present purposes through a few constant parameters. Use will be made here of results from an analysis by Aldredge (1990) which provides these equations and parameters fully. The analysis employs the theory of Clavin & Garcia-Ybarra (1983) but retains nonlinear terms of order δ^2 that they neglected. Their theory treats the specific heat and Prandtl and Schmidt numbers as constant for flames having reactants that can be characterized by a single diffusion coefficient and addresses one-step, Arrhenius chemistry having a large Zel'dovich number β (as defined in Williams 1985) but otherwise allows arbitrary variations in properties through the flame. Removal of these assumptions, for example by introducing more realistic chemistry, seems likely to usually leave the general forms of the jump and evolution equations unchanged but to modify the expressions for the parameters appearing therein (Clavin 1985). Thus there is reason to believe that the formulation can be applied with some confidence to real flames.

On each side of the discontinuity in figure 1 are regions of hydrodynamic adjustment, of characteristic length l. Since the Mach number is low, the temperature, density and coefficients of viscosity remain constant in each of these regions. Variations of the flow field through these regions were not addressed in the earliest studies along these lines (Clavin & Williams 1979, 1982) but have been shown to be of major significance to the dynamics and stability of wrinkled laminar flames (Pelce & Clavin 1982). The analysis of Searby & Clavin (1986), on which the present work is based, is focused primarily on influences occurring in these regions of hydrodynamic adjustment. Since our development pertains largely to these regions, scalings will be introduced to render variables therein of order unity.

Since the incompressible Navier–Stokes equations describe the flow in the hydrodynamic regions, the problem addressed essentially involves two Navier–Stokes fluids of different densities and viscosities with a moving boundary between them. The non-linearity of the inertial terms complicates Navier–Stokes analyses. Therefore, for analytical tractability Searby & Clavin (1986) restricted their attention to the linearized Navier–Stokes equations. We too introduce the

expansion for small amplitudes of velocity fluctuations, thereby restricting the analysis to weak turbulence ($\delta \ll 1$). In the terminology employed for grid turbulence, the applicability of the results is limited to turbulence in the final stages of decay (Batchelor 1956; Clavin & Williams 1979, 1982) if δ is of order ϵ or smaller. We may, however, formally avoid this restriction by taking $\epsilon \ll \delta$. An objective is to consider how departures from the low-intensity limit begin.

The well-known hydrodynamic instability of premixed laminar flames (Williams 1985) predicted by Darrius and Landau restricts the problems amenable to our analysis. The approach applies only for flames that are intrinsically stable. Diffusive–thermal effects can introduce the needed stability only for wavelengths that are not too large. Another stabilizing influence is needed for longer wavelengths, and this is provided conveniently by buoyancy for flames propagating downward (Pelcé & Clavin 1982). Therefore the analysis presumes that the combination of buoyant and diffusive-thermal effects serves to stabilize the hydrodynamic instability for all wavelengths. An excellent review is available (Clavin 1985) giving a more thorough discussion of these aspects.

A stationary problem is considered in which the reactants flow upward in the $\bar{x}$-direction (figure 1). Homogeneity in transverse directions is hypothesized in addition to the stationarity. The average location of the flame discontinuity is placed at $\bar{x} = 0$ in the laboratory frame, with the reactants flowing from $\bar{x} = -\infty$ and the products flowing to $\bar{x} = +\infty$. The scalings and formulation are summarized in the following section. Expansions, Fourier decompositions, and results concerning flame properties are then developed in subsequent sections.

2. Formulation

Since within the context of the analysis departures of velocities from laminar-flame velocities are small, it is convenient to use the laminar burning velocity V measured in the unburnt gas and a representative turbulence scale l to non-dimensionalize distance and time coordinates. Thus $\bar{t}$ denotes time in units of l/V, $\bar{x}$ the streamwise distance in units of l, and $\bar{y}$ the two-dimensional transverse coordinate vector in units of l. Streamwise and transverse velocities in units of V, in the laboratory frame, are denoted by u and v, respectively. The wrinkled-flame location (in units of l) is defined by $\bar{x} = \bar{f}(\bar{y}, \bar{t})$, which is assumed to be single-valued, thereby limiting the permissible extent of wrinkling (Williams 1985). The non-dimensional departure of the pressure from that of the undisturbed, planar laminar flame (located at $\bar{x} = 0$ in the gravitational field) will be denoted by p; here the non-dimensionalization is achieved through division by $\rho_- V^2$, where ρ_- is the density of the fresh mixture. The conservation equations will be written in a coordinate system (x, y, t) that moves with the flame; specifically, $x = \bar{x} - \bar{f}$, $y = \bar{y}$ and $t = \bar{t}$, and the definition $f(y, t) \equiv \bar{f}(\bar{y}, \bar{t})$ is introduced. The basic forms of the expansions to be sought are then

$$\left.\begin{aligned} u &\sim u_0 + \delta u_1 + \delta^2 u_2 + \ldots, \\ v &\sim \delta v_1 + \delta^2 v_2 + \ldots, \\ p &\sim \delta p_1 + \delta^2 p_2 + \ldots, \\ f &\sim \delta f_1 + \delta^2 f_2 + \ldots, \end{aligned}\right\} \tag{1}$$

where the functions of (x, y, t) multiplying the powers of the primary expansion parameter δ also will depend on ϵ and other parameters. The precise definition of δ

is taken to be the relative intensity that would exist at $\bar{x} = 0$ if the flame were not lit.

The complete conservation equations for flow in the hydrodynamic regions can be written as (Aldredge 1990)

$$\frac{\partial}{\partial x}\left(u - \frac{\partial f}{\partial t} - \boldsymbol{v}\cdot\boldsymbol{\nabla} f\right) + \boldsymbol{\nabla}\cdot\boldsymbol{v} = \boldsymbol{0}, \tag{2}$$

$$\frac{\partial u}{\partial t} + \left(u - \frac{\partial f}{\partial t} - \boldsymbol{v}\cdot\boldsymbol{\nabla} f\right)\frac{\partial u}{\partial x} + \boldsymbol{v}\cdot\boldsymbol{\nabla} u = u_0\left(-\frac{\partial p}{\partial x} + \epsilon Prs\,\Delta u\right), \tag{3}$$

$$\frac{\partial \boldsymbol{v}}{\partial t} + \left(u - \frac{\partial f}{\partial t} - \boldsymbol{v}\cdot\boldsymbol{\nabla} f\right)\frac{\partial \boldsymbol{v}}{\partial x} + (\boldsymbol{v}\cdot\boldsymbol{\nabla})\,\boldsymbol{v} = u_0\left(-\boldsymbol{\nabla} p + \frac{\partial p}{\partial x}\boldsymbol{\nabla} f + \epsilon Prs\Delta \boldsymbol{v}\right) - Ri\,\boldsymbol{\nabla} f. \tag{4}$$

Here $\boldsymbol{\nabla}$ denotes the nondimensional transverse gradient involving derivatives with respect to components of $\boldsymbol{y}$, and p is the departure of the hydrostatic pressure from the quantity $-xRi/u_0$ (which in the laboratory frame varies with time and the transverse coordinates), where the Richardson number Ri is defined below. The Laplacian operator in the moving coordinates becomes

$$\Delta = [1 + |\boldsymbol{\nabla} f|^2]\frac{\partial^2}{\partial x^2} + \nabla^2 - 2\boldsymbol{\nabla} f\cdot\boldsymbol{\nabla}\frac{\partial}{\partial x} - \nabla^2 f\frac{\partial}{\partial x}. \tag{5}$$

In general, the subscripts $-$ and $+$ will identify quantities evaluated at $x = 0$ immediately on the upstream and downstream sides of the flame, respectively; for properties such as the density, ρ, the coefficient of viscosity, μ, and the thermal diffusivity, α, which remain constant throughout each hydrodynamic zone, these subscripts are equivalent to signifying evaluation in the burnt products leaving the turbulent flame ($x \to \infty$) and in the fresh reactants entering it ($x \to -\infty$), respectively. In the definition $\epsilon \equiv d/l$, the thermal diffusivity of the unburnt mixture is employed to specify the thickness d, so that $d = \alpha_-/V$. The (constant) Prandtl number $Pr \equiv \mu/(\rho\alpha)$ then appears in (3) and (4), since the Reynolds number based on V and the integral scale l is $(\epsilon Pr)^{-1}$. The turbulence Reynolds number, based on the fluctuation velocity and the integral scale, is then seen to be of order δ/ϵ in this analysis (with Pr of order unity) and thus may be of order unity, for example. The definition $s \equiv \mu/\mu_-$ has been introduced here, so that $s = 1$ in the fresh mixture, and $s = S \equiv \mu_+/\mu_- \geqslant 1$ in the burnt gas. Use has also been made of the zero-order solution, $u_0 = 1$ in the upstream region and $u_0 = R \equiv \rho_-/\rho_+ \geqslant 1$ downstream. Finally, in (4) the Richardson number $Ri = gl/V^2$ has been introduced, where g is the acceleration due to gravity; this is found more convenient than its reciprocal, the Froude number, and it will be treated as being of order unity. Worthy of re-emphasis is the fact that (2), (3) and (4) are exact in that they have not involved any expansions. Also, it is noted again that u and $\boldsymbol{v}$ in these equations are measured in the laboratory reference frame and not in the moving coordinate system.

The jump conditions to be applied at $x = 0$ are (Aldredge 1990)

$$u_+ - u_- = (R-1)\,[1 - \tfrac{1}{2}|\boldsymbol{\nabla} f|^2] - \epsilon(R-1)\,(L-J)\,[(\boldsymbol{\nabla}\cdot\boldsymbol{v})_- + \nabla^2 f] + O(\delta^4, \epsilon\delta^2, \epsilon^2\delta, \delta\beta^{-1}), \tag{6}$$

$$\boldsymbol{v}_+ - \boldsymbol{v}_- = -(R-1)\,\boldsymbol{\nabla} f + \epsilon J\frac{R-1}{R}\left[\left(\frac{\partial \boldsymbol{v}}{\partial t}\right)_- + \boldsymbol{\nabla}\frac{\partial f}{\partial t} + Ri\,\boldsymbol{\nabla} f\right]$$

$$+ \epsilon Pr\,S\left[\left(\frac{\partial \boldsymbol{v}}{\partial x}\right)_+ - \left(\frac{\partial \boldsymbol{v}}{\partial x}\right)_-\right] + \epsilon Pr\,(S-1)\left[(\boldsymbol{\nabla} u)_- + \left(\frac{\partial \boldsymbol{v}}{\partial x}\right)_-\right] + O(\delta^3, \epsilon\delta^2, \epsilon^2\delta, \delta\beta^{-1}), \tag{7}$$

$$p_+ - p_- = 2\epsilon(R-1)(L-J)[(\nabla\cdot\boldsymbol{v})_- + \nabla^2 f] + \epsilon J\frac{R-1}{R}\left(\frac{\partial u}{\partial t}\right)_- + \epsilon(R-1)(1-Pr-Pr')S\nabla^2 f$$
$$+\epsilon(R-1)H\nabla^2 f + 2\epsilon Pr(S-1)\left(\frac{\partial u}{\partial x}\right)_- + \epsilon(Pr+Pr')S\left[\left(\frac{\partial u}{\partial x}\right)_+ - \left(\frac{\partial u}{\partial x}\right)_-\right]$$
$$+O(\epsilon\delta^2, \epsilon^2\delta, \delta\beta^{-1}), \tag{8}$$

$$\frac{\partial f}{\partial t} = (u_- - 1) - \boldsymbol{v}_-\cdot\nabla f + \epsilon L[(\nabla\cdot\boldsymbol{v})_- + \nabla^2 f] - \tfrac{1}{2}|\nabla f|^2 + O(\delta^4, \epsilon\delta^2, \epsilon^2\delta, \delta\beta^{-1}). \tag{9}$$

Appearing in (8) is the second Prandtl number, Pr', defined as $Pr' \equiv (\kappa + \frac{1}{3}\mu)/(\rho\alpha)$, where κ is the coefficient of bulk viscosity. Additional, dependent parameters arise in (5)–(9) and are defined as

$$J \equiv \int_0^1 \frac{sR}{1+(R-1)\theta}\,\mathrm{d}\theta, \tag{10a}$$

as the non-dimensional Markstein length

$$L \equiv J - \tfrac{1}{2}\beta(Le-1)\int_0^1 \frac{s\ln\theta}{1+(R-1)\theta}\,\mathrm{d}\theta, \tag{10b}$$

and as

$$H \equiv (2Pr-1)\int_0^1 (S-s)\,\mathrm{d}\theta, \tag{10c}$$

where the variable of integration is the non-dimensional temperature, $\theta = (T-T_-)/(T_+-T_-)$. The Lewis number $Le \equiv \alpha/D_\mathrm{m}$ (where D_m is the molecular diffusion coefficient) and the Zel'dovich number β are seen to occur only in the non-dimensional Markstein length. The origins and meanings of these evolution equations and jump conditions have been discussed in the literature (Pelce & Clavin, 1982; Clavin & Garcia-Ybarra 1983; Clavin 1985). The flame-structure hypotheses (and results of activation-energy asymptotics) affect only the formula for L, so long as there exists an inert preheat zone in the flame. The equations employed by Searby & Clavin (1986) are the linear versions of (2)–(9).

In (6)–(9) the terms $(\nabla\cdot\boldsymbol{v})_-$ and $\nabla^2 f$ represent flame stretch and flame curvature, respectively, these influences arise through the internal structure of the flame and therefore always appear multiplied by ϵ and by one of the parameters in (10). In (9) the terms $\boldsymbol{v}\cdot\nabla f$ and $|\nabla f|^2$ represent transverse convection and flame tilt, respectively, both of which tend to reduce $\partial f/\partial t$ through kinematic and geometric effects. The terms multiplied by $R-1$ are gas-expansion effects that vanish in constant-density flows. Further discussion may be found in Pelce & Clavin (1982), Clavin & Garcia-Ybarra (1983), Williams (1985), Clavin (1985) and Aldredge (1990).

3. Expansion to second order

The form of the expansions sought has been given in (1). Expansion of (2)–(5) up to order δ^2 gives

$$\frac{\partial u_1}{\partial x} + \nabla\cdot\boldsymbol{v}_1 = 0, \tag{11a}$$

$$u_0^{-1}\frac{\partial u_1}{\partial t} + \frac{\partial u_1}{\partial x} = -\frac{\partial p_1}{\partial x} + \epsilon Prs\left(\frac{\partial^2 u_1}{\partial x^2} + \nabla^2 u_1\right), \tag{11b}$$

$$u_0^{-1}\frac{\partial \boldsymbol{v}_1}{\partial t} + \frac{\partial \boldsymbol{v}_1}{\partial x} = -\nabla p_1 - u_0^{-1}Ri\,\nabla f_1 + \epsilon Prs\left(\frac{\partial^2 \boldsymbol{v}_1}{\partial x^2} + \nabla^2 \boldsymbol{v}_1\right) \tag{11c}$$

at order δ and

$$\frac{\partial u_2}{\partial x}+\nabla\cdot\boldsymbol{v}_2=\frac{\partial \boldsymbol{v}_1}{\partial x}\cdot\nabla f_1, \tag{12a}$$

$$u_0^{-1}\frac{\partial u_2}{\partial t}+\frac{\partial u_2}{\partial x}=-\frac{\partial p_2}{\partial x}+u_0^{-1}\left(\frac{\partial f_1}{\partial t}-u_1\right)\frac{\partial u_1}{\partial x}-u_0^{-1}\boldsymbol{v}_1\cdot\nabla u_1$$
$$+\epsilon Pr\,s\left(\frac{\partial^2 u_2}{\partial x^2}+\nabla^2 u_2\right)-\epsilon Pr\,s\,[2(\nabla f_1)\cdot\nabla+(\nabla^2 f_1)]\frac{\partial u_1}{\partial x}, \tag{12b}$$

$$u_0^{-1}\frac{\partial \boldsymbol{v}_2}{\partial t}+\frac{\partial \boldsymbol{v}_2}{\partial x}=-\nabla p_2-u_0^{-1}Ri\,\nabla f_2+\frac{\partial p_1}{\partial x}\nabla f_1+u_0^{-1}\left(\frac{\partial f_1}{\partial t}-u_1\right)\frac{\partial \boldsymbol{v}_1}{\partial x}-u_0^{-1}(\boldsymbol{v}_1\cdot\nabla)\,\boldsymbol{v}_1$$
$$+\epsilon Pr\,s\left(\frac{\partial^2 \boldsymbol{v}_2}{\partial x^2}+\nabla^2\boldsymbol{v}_2\right)-\epsilon Pr\,s\,[2(\nabla f_1)\cdot\nabla+(\nabla^2 f_1)]\frac{\partial \boldsymbol{v}_1}{\partial x} \tag{12c}$$

at order δ^2. Adding the longitudinal derivative of (11b) to the transverse divergence of (11c), then employing continuity, (11a), gives a Poisson equation for the pressure p_1, namely,

$$\partial^2 p_1/\partial x^2+\nabla^2 p_1=-u_0^{-1}Ri\,\nabla^2 f_1. \tag{13}$$

Similarly, solving (12) for p_2 gives

$$\partial^2 p_2/\partial x^2+\nabla^2 p_2=-u_0^{-1}Ri\,\nabla^2 f_2+N_2(x,y,t), \tag{14}$$

where the nonlinear terms, denoted by $N_2(x,y,t)$ are known from the solution of (11) and are given by

$$N_2(x,y,t)=2(\nabla f_1)\cdot\nabla\left(\frac{\partial p_1}{\partial x}\right)+\frac{\partial p_1}{\partial x}\nabla^2 f_1-u_0^{-1}\left[\left(\frac{\partial u_1}{\partial x}\right)^2+(\nabla\boldsymbol{v}_1):(\nabla\boldsymbol{v}_1)^T+2\frac{\partial \boldsymbol{v}_1}{\partial x}\cdot\nabla u_1\right]. \tag{15}$$

The symbol : denotes double contraction of the dyadics. Equations (13) and (14) may be viewed as convenient replacements for (11a) and (12a), for example, if desired.

Introduction of (1) into (6)–(9) and collection of like powers of δ gives

$$u_{1+}=u_{1-}-\epsilon(R-1)\,(L-J)\,[(\nabla\cdot\boldsymbol{v}_1)_-+\nabla^2 f_1]+O(\epsilon^2,\beta^{-1}), \tag{16a}$$

$$\boldsymbol{v}_{1+}=\boldsymbol{v}_{1-}-(R-1)\,\nabla f_1+\epsilon J\,\frac{R-1}{R}\left[\left(\frac{\partial \boldsymbol{v}_1}{\partial t}\right)_-+\nabla\frac{\partial f_1}{\partial t}+Ri\,\nabla f_1\right]$$
$$+\epsilon Pr\,S\left[\left(\frac{\partial \boldsymbol{v}_1}{\partial x}\right)_+-\left(\frac{\partial \boldsymbol{v}_1}{\partial x}\right)_-\right]+\epsilon Pr\,(S-1)\left[\nabla u_{1-}+\left(\frac{\partial \boldsymbol{v}_1}{\partial x}\right)_-\right]+O(\epsilon^2,\beta^{-1}), \tag{16b}$$

$$p_{1+}=p_{1-}+2\epsilon(R-1)\,(L-J)\,[(\nabla\cdot\boldsymbol{v}_1)_-+\nabla^2 f_1]+\epsilon J\frac{R-1}{R}\left(\frac{\partial u_1}{\partial t}\right)_-$$
$$+\epsilon(R-1)\,(1-Pr-Pr')\,S\nabla^2 f_1+\epsilon(R-1)\,H\nabla^2 f_1+2\epsilon Pr(S-1)\left(\frac{\partial u_1}{\partial x}\right)_-$$
$$+\epsilon(Pr+Pr')\,S\left[\left(\frac{\partial u_1}{\partial x}\right)_+-\left(\frac{\partial u_1}{\partial x}\right)_-\right]+O(\epsilon^2,\beta^{-1}), \tag{16c}$$

$$\frac{\partial f_1}{\partial t}=u_{1-}+\epsilon L[(\nabla\cdot\boldsymbol{v}_1)_-+\nabla^2 f_1]+O(\epsilon^2,\beta^{-1}) \tag{16d}$$

at order δ, and

$$\left.\begin{aligned} u_{2+} &= u_{2-} - \tfrac{1}{2}(R-1)\,|\nabla f_1|^2 + O(\epsilon, \beta^{-1}), \\ \boldsymbol{v}_{2+} &= \boldsymbol{v}_{2-} - (R-1)\,\nabla f_2 + O(\epsilon, \beta^{-1}), \\ p_{2+} &= p_{2-} + O(\epsilon, \beta^{-1}), \\ \frac{\partial f_2}{\partial t} &= u_{2-} - \boldsymbol{v}_{1-} \cdot \nabla f_1 - \tfrac{1}{2}|\nabla f_1|^2 + O(\epsilon, \beta^{-1}) \end{aligned}\right\} \tag{17}$$

at order δ^2. The first-order problem defined by (11) and (16) is linear and is solved conveniently by Fourier decomposition. The results may then be used to solve in a similar manner the second-order problem defined by (12) and (17). The ordering restrictions shown in (16) and (17) are dictated by those given in (6)–(9); in particular, all terms of order ϵ have been excluded from (17) because some terms of order $\epsilon\delta^2$ were neglected in (6)–(9). Terms of order ϵ in (17) that would arise from the terms actually appearing in (6)–(9) can easily be included in (17), maintaining the same order of accuracy, if they are helpful in obtaining solutions.

It should be noted that in the calculations made here only the development to leading order as defined by (11) and (16) is needed (cf. §5). The formulation of the second-order problem is added to provide a framework for future analyses of higher-order, nonlinear effects of the coupling between the flame front and the turbulent flow. In the Conclusion of this investigation we discuss, qualitatively, expected modifications to the leading-order theory from the non-linearities.

4. Fourier decomposition

Since the first-order problem is linear, transversely homogeneous and stationary, it is convenient to introduce the Fourier decompositions

$$\begin{bmatrix} U_1 \\ V_1 \\ P_1 \\ F_1 \end{bmatrix} = \int_{-\infty}^{\infty}\int_{-\infty}^{\infty}\int_{-\infty}^{\infty} \begin{bmatrix} u_1 \\ v_1 \\ p_1 \\ f_1 \end{bmatrix} \mathrm{e}^{-\mathrm{i}(\omega t + \boldsymbol{k}\cdot\boldsymbol{y})} \frac{\mathrm{d}\boldsymbol{y}\,\mathrm{d}t}{(2\pi)^3} \tag{18}$$

which render U_1, V_1 and P_1 functions of x, ω (frequency) and $\boldsymbol{k}$ (wavenumber) and F_1 a function of ω and $\boldsymbol{k}$. The inverse transforms give

$$\begin{bmatrix} u_1 \\ v_1 \\ p_1 \\ f_1 \end{bmatrix} = \int_{-\infty}^{\infty}\int_{-\infty}^{\infty}\int_{-\infty}^{\infty} \begin{bmatrix} U_1 \\ V_1 \\ P_1 \\ F_1 \end{bmatrix} \mathrm{e}^{\mathrm{i}(\omega t + \boldsymbol{k}\cdot\boldsymbol{y})}\,\mathrm{d}\boldsymbol{k}\,\mathrm{d}\omega. \tag{19}$$

The conservation equations to be solved at the first order may be taken to be (11*b*, *c*) and (13), the transforms of which are

$$\left.\begin{aligned} \frac{\mathrm{i}\omega}{u_0}U_1 + \frac{\partial U_1}{\partial x} &= -\frac{\partial P_1}{\partial x} + \epsilon Pr\,s\left(\frac{\partial^2 U_1}{\partial x^2} - k^2 U_1\right), \\ \frac{\mathrm{i}\omega}{u_0}V_1 + \frac{\partial V_1}{\partial x} &= -\mathrm{i}kP_1 - \frac{\mathrm{i}k}{u_0}Ri\,F_1 + \epsilon Pr\,s\left(\frac{\partial^2 V_1}{\partial x^2} - k^2 V_1\right), \\ \frac{\partial^2 P_1}{\partial x^2} - k^2 P_1 &= \frac{k^2}{u_0}Ri\,F_1 \end{aligned}\right\} \tag{20}$$

for $x < 0$ and $x > 0$, where $k \equiv |\boldsymbol{k}|$. The transforms of (16),

$$U_{1+} = U_{1-} - \epsilon(R-1)(L-J)(\mathrm{i}\boldsymbol{k}\cdot\boldsymbol{V}_{1-} - k^2F_1), \tag{21a}$$

$$\boldsymbol{V}_{1+} = \boldsymbol{V}_{1-} - (R-1)\,\mathrm{i}\boldsymbol{k}F_1 + \epsilon\frac{J}{R}(R-1)(\mathrm{i}\omega\boldsymbol{V}_{1-} - \boldsymbol{k}\omega F_1 + \mathrm{i}\boldsymbol{k}RiF_1) + \epsilon Pr\left[S\left(\frac{\partial \boldsymbol{V}_1}{\partial x}\right)_+ - \left(\frac{\partial \boldsymbol{V}_1}{\partial x}\right)_- + \mathrm{i}\boldsymbol{k}(S-1)U_{1-}\right], \tag{21b}$$

$$P_{1+} = P_{1-} + 2\epsilon(R-1)(L-J)(\mathrm{i}\boldsymbol{k}\cdot\boldsymbol{V}_{1-} - k^2F_1) + \epsilon\,\mathrm{i}\omega\frac{J}{R}(R-1)U_{1-} + \epsilon(R-1)[(1-Pr-Pr')S-H]k^2F_1 + \epsilon\left\{(Pr+Pr')S\left(\frac{\partial U_1}{\partial x}\right)_+ + [(Pr-Pr')S-2Pr]\left(\frac{\partial U_1}{\partial x}\right)_-\right\}, \tag{21c}$$

$$\mathrm{i}\omega F_1 = U_{1-} + \epsilon L(\mathrm{i}\boldsymbol{k}\cdot\boldsymbol{V}_{1-} - k^2F_1) \tag{21d}$$

are to be applied at $x = 0$.

Solutions to this linear problem are to be sought in terms of responses to fluctuation velocities imposed from upstream, given by,

$$U_1 = U_{\mathrm{e}}\mathrm{e}^{-[\mathrm{i}\omega+\epsilon Pr(\omega^2+k^2)]x}, \quad \boldsymbol{V}_1 = \boldsymbol{V}_{\mathrm{e}}\mathrm{e}^{-[\mathrm{i}\omega+\epsilon Pr(\omega^2+k^2)]x}, \tag{22}$$

where $\boldsymbol{V}_{\mathrm{e}}(\boldsymbol{k},\omega)$ is arbitrary, while U_{e} is determined from the transform of the continuity equation, (11a), namely,

$$\partial U_1/\partial x = -\mathrm{i}\boldsymbol{k}\cdot\boldsymbol{V}_1, \tag{23}$$

which gives $U_{\mathrm{e}} = \boldsymbol{k}\cdot\boldsymbol{V}_{\mathrm{e}}/[\omega - \mathrm{i}\epsilon Pr(\omega^2+k^2)]$. The subscript e refers to the excitation field in a transfer-function interpretation (Searby & Clavin 1986); the form shown in (22) has been selected to be consistent with the conservation equations applicable in the absence of the flame, with the iω-term representing the turbulence and the ϵ-term accounting for its decay, which is slow in the x-scale for small ϵ. The solutions to (2) that approach (22) as $x \to -\infty$ and remain bounded as $x \to \infty$ can be written in the form

$$P_1 = P_-\mathrm{e}^{kx} - RiF_1, \quad x < 0; \qquad P_1 = P_+\mathrm{e}^{-kx} - (Ri/R)F_1, \quad x > 0, \tag{24a}$$

$$U_1 = U_{\mathrm{e}}\mathrm{e}^{-[\mathrm{i}\omega+\epsilon Pr(\omega^2+k^2)]x} - kP_-\mathrm{e}^{kx}/(k+\mathrm{i}\omega), \quad x < 0, \tag{24b}$$

$$U_1 = U_{\mathrm{f}}\mathrm{e}^{-\{\mathrm{i}\omega/R+\epsilon Pr\,S[(\omega/R)^2+k^2]\}x} - kP_+\mathrm{e}^{-kx}/(k-\mathrm{i}\omega/R), \quad x > 0, \tag{24c}$$

$$\boldsymbol{V}_1 = \boldsymbol{V}_{\mathrm{e}}\mathrm{e}^{-[\mathrm{i}\omega+\epsilon Pr(\omega^2+k^2)]x} - \mathrm{i}\boldsymbol{k}P_-\mathrm{e}^{kx}/(k+\mathrm{i}\omega), \quad x < 0, \tag{24d}$$

$$\boldsymbol{V}_1 = \boldsymbol{V}_{\mathrm{f}}\mathrm{e}^{-\{\mathrm{i}\omega/R+\epsilon Pr\,S[(\omega/R)^2+k^2]\}x} + \mathrm{i}\boldsymbol{k}P_+\mathrm{e}^{-kx}/(k-\mathrm{i}\omega/R), \quad x > 0, \tag{24e}$$

in which the quantities $\boldsymbol{V}_{\mathrm{f}}$, P_-, P_+ and F_1 are functions of $\boldsymbol{k}$ and ω that are obtained by applying the jump conditions, (21), while U_{f} is determined from the continuity equation, (23). Transforms of interest from these solutions are those of the wrinkled-flame displacement, F_1, and velocity, $\mathrm{i}\omega F_1$, the velocity perturbations just upstream from the wrinkled flame, $U_- \equiv U_{\mathrm{e}} - kP_-/(k+\mathrm{i}\omega)$ and $\boldsymbol{V}_- \equiv \boldsymbol{V}_{\mathrm{e}} - \mathrm{i}\boldsymbol{k}P_-/(k+\mathrm{i}\omega)$, the velocity perturbations just downstream from the wrinkled flame, $U_+ \equiv U_{\mathrm{f}} - kP_+/(k-\mathrm{i}\omega/R)$ and $\boldsymbol{V}_+ \equiv \boldsymbol{V}_{\mathrm{f}} + \mathrm{i}\boldsymbol{k}P_+/(k-\mathrm{i}\omega/R)$, the pressure perturbations measured in the laboratory reference frame at $\bar{x} = 0$, P_- and P_+, and the velocity perturbations in the final outgoing product flow, which have been denoted as U_{f} and $\boldsymbol{V}_{\mathrm{f}}$.

Application of the jump conditions in (21) to the solutions in (24) reveals that

$$F_1 = 2(k+\mathrm{i}\omega)\,(1+\epsilon\{k[(R-1)\,(L-J)-Pr\,(S-1)]+\mathrm{i}\omega L\})\,U_e/D, \tag{25a}$$

$$\begin{aligned}P_- = (k+\mathrm{i}\omega)\Bigg[&\omega^2\left\{\frac{R-1}{R}+\epsilon k\left[2(R-1)\,(L-J)+\frac{(R-1)\,J}{R}-2Pr(S-1)\right]\right\}\\&+k(R-1)\left\{\frac{Ri}{R}-k\left[1-\frac{\epsilon Ri}{R}J\right]+\epsilon k^2[H+S+2(L-J)]\right\}\\&+\epsilon\mathrm{i}\omega\left\{\frac{(R-1)\,L(kRi+\omega^2)}{R}+k^2[2Pr(S-1)-(R-1)\,L]\right\}\Bigg]\frac{U_e}{kD},\end{aligned} \tag{25b}$$

$$\begin{aligned}P_+ = (k+\mathrm{i}\omega)\Bigg[&\frac{\omega^2\{R-1-\epsilon k[(R-1)\,(2L-J)-2Pr(S-1)]\}}{R}\\&-k(R-1)\left\{\frac{Ri}{R}+k\left[1-\frac{\epsilon Ri}{R}J\right]+\epsilon k^2[H-2Pr(S-1)+S+2R(L-J)]\right\}\\&-\epsilon\mathrm{i}\omega\{(R-1)\,L(kRi-\omega^2)/R+k^2[(R-1)\,L+2Pr(S-1)]\}\Bigg]\frac{U_e}{kD},\end{aligned} \tag{25c}$$

$$\begin{aligned}U_f = (k+\mathrm{i}\omega)\Bigg(&\omega^2\left\{\frac{R+1}{R}+\epsilon k(R-1)\left[(L-J)-\frac{2J}{R}\right]\right\}-(R-1)\,k\left\{\frac{Ri}{R}+k[1+\epsilon Ri(L-J)]\right\}\\&+\epsilon k^3\{J(R+1)-(L-J)\,R(R-3)+(R-1)\,[2Pr(S-1)-(S+H)]\}\\&+\mathrm{i}\omega\left[k\left\{2-J(\epsilon Ri)\left[\frac{R-1}{R}\right]^2\right\}-\epsilon k^2\left[\frac{J(R^2+1)}{R}+2(L-J)\right]\right.\\&\left.+\frac{\epsilon\omega^2J(R^2-1)}{R^2}\right]\Bigg)\frac{U_e}{(k-\mathrm{i}\omega/R)\,D},\end{aligned} \tag{25d}$$

$$\left.\begin{aligned}V_f &= A(k,\omega)\,\mathrm{i}\boldsymbol{k}U_e+B(\omega)\boldsymbol{V}_e,\\A(k,\omega) &= (R-1)\left[-1+\frac{\epsilon JRi}{R}+\frac{\epsilon\mathrm{i}\omega(J-Pr\,S)}{R}\right]\frac{F_1}{U_e}\\&\quad-\left\{1+\epsilon kPr(S-2)+\frac{\epsilon\mathrm{i}\omega[(R-1)\,J-Pr\,S]}{R}\right\}\frac{P_-/U_e}{k+\mathrm{i}\omega}\\&\quad-\left[\frac{1}{k-\mathrm{i}\omega/R}+\epsilon Pr\,S\right]\frac{P_+}{U_e}+\epsilon Pr(S-1),\\B(\omega) &= 1+\epsilon\,\mathrm{i}\omega[J(R-1)/R+Pr(1-S/R)],\end{aligned}\right\} \tag{25e}$$

where the inverse transfer function D (the vanishing of which would provide the dispersion relation) is defined as

$$\begin{aligned}D(\boldsymbol{k},\omega) \equiv &-\frac{\omega^2[R+1+\epsilon k(R-1)\,(L-J)]}{R}+2\mathrm{i}\omega k\left\{1+\epsilon kR\left[L-\frac{(R-1)\,J}{R}\right]\right\}\\&+k(R-1)\left\{\frac{Ri}{R}-k\left[1+\frac{\epsilon Ri(L-J)}{R}\right]+\epsilon k^2\left[S+\frac{(3R-1)\,L}{R-1}-2J+H\right]\right\}.\end{aligned} \tag{26}$$

The primary purpose of introducing $\epsilon > 0$ and $Ri > 0$ into the problem has been to render the planar laminar flame stable, that is, to prevent the equation $D = 0$ from having any solutions for real, non-negative values of k that give a negative imaginary part for ω. This function of ϵ and Ri is served by (26) (Clavin & Garcia-Ybarra 1983; Clavin 1985; Searby & Clavin 1986), which is the same as the corresponding formula

of Searby & Clavin (1986). The appearance of ϵ and Ri elsewhere in (25) therefore is of secondary interest, and these terms may be neglected in presenting results for large-scale turbulence in weak gravitational fields.

5. Flame-speed calculations

The non-dimensional turbulent flame speed, denoted here as $1+u_{\mathrm{T}}$, is the average velocity of the incoming flow measured in the laboratory reference frame. This may be evaluated at any value of $\bar{x}$ but is conveniently calculated at $\bar{x}=0$ from the Taylor expansion $u_-+(\partial u/\partial x)_- f+\ldots$. Use of stationarity and transverse homogeneity in the ensemble average of (9) then gives

$$u_{\mathrm{T}} = \tfrac{1}{2}\overline{|\nabla f|^2} + O(\delta^4, \epsilon\delta^2, \epsilon^2\delta, \delta\beta^{-1}), \tag{27}$$

where the overbar denotes the average, which here may be calculated from knowledge of ∇f_1 and of the two-point, two-time correlation function of the excitation field, defined as

$$g_u(|\boldsymbol{y}_2-\boldsymbol{y}_1|, |t_2-t_1|) \equiv \overline{u_{\mathrm{e}}(\boldsymbol{y}_1, t_1)\, u_{\mathrm{e}}(\boldsymbol{y}_2, t_2)}/\delta^2 \tag{28}$$

for transversely isotropic (axisymmetric) turbulence.

It follows from (18) and (19) and the convolution theorem for Fourier transforms that if the Fourier transform of ∇f_1 is given as the product of U_{e} and a transfer function $\boldsymbol{Q}_{\nabla f}$ such that $\mathrm{i}\boldsymbol{k}F_1(\boldsymbol{k},\omega) = \boldsymbol{Q}_{\nabla f}(\boldsymbol{k},\omega)\, U_{\mathrm{e}}(\boldsymbol{k},\omega)$ then

$$\nabla f_1(\boldsymbol{y}, t) = \int_{-\infty}^{\infty} \mathrm{d}\boldsymbol{y}_1 \int_{-\infty}^{\infty} \mathrm{d}t_1\, \boldsymbol{q}_{\nabla f}(\boldsymbol{y}_1, t_1)\, u_{\mathrm{e}}(\boldsymbol{y}-\boldsymbol{y}_1, t-t_1)/(2\pi)^3,$$

where $\boldsymbol{q}_{\nabla f}$ is the inverse Fourier transform of $\boldsymbol{Q}_{\nabla f}$. Squaring this result and taking an ensemble average gives

$$\overline{|\nabla f_1|^2} = \delta^2 \int_{-\infty}^{\infty} \mathrm{d}\boldsymbol{y}_1 \int_{-\infty}^{\infty} \mathrm{d}t_1 \int_{-\infty}^{\infty} \mathrm{d}\boldsymbol{y}_2 \int_{-\infty}^{\infty} \mathrm{d}t_2\, \boldsymbol{q}_{\nabla f}(\boldsymbol{y}_1, t_1)\cdot \boldsymbol{q}_{\nabla f}(\boldsymbol{y}_2, t_2)\, g_u(|\boldsymbol{y}_2-\boldsymbol{y}_1|, |t_2-t_1|)/(2\pi)^6,$$

in which the new variables $\boldsymbol{y}=\boldsymbol{y}_2-\boldsymbol{y}_1$ and $t=t_2-t_1$ may be introduced and the Parseval-type identity

$$\int_{-\infty}^{\infty} \mathrm{d}\boldsymbol{y}_1 \int_{-\infty}^{\infty} \mathrm{d}t_1\, \boldsymbol{q}_{\nabla f}(\boldsymbol{y}_1, t_1)\cdot \boldsymbol{q}_{\nabla f}(\boldsymbol{y}+\boldsymbol{y}_1, t+t_1) \equiv (2\pi)^3 \int_{-\infty}^{\infty} \mathrm{d}\boldsymbol{k} \int_{-\infty}^{\infty} \mathrm{d}\omega\, |\boldsymbol{Q}_{\nabla f}(\boldsymbol{k},\omega)|^2\, \mathrm{e}^{-\mathrm{i}(\omega t+\boldsymbol{k}\cdot\boldsymbol{y})}$$

employed to obtain

$$\overline{|\nabla f_1|^2} = \delta^2 \int_{-\infty}^{\infty} \mathrm{d}\boldsymbol{k} \int_{-\infty}^{\infty} \mathrm{d}\omega\, |\boldsymbol{Q}_{\nabla f}(\boldsymbol{k},\omega)|^2 G_u(\boldsymbol{k},\omega) \tag{29}$$

at the lowest order, where $G_u(\boldsymbol{k},\omega)$ is the Fourier transform of $g_u(|\boldsymbol{y}|, |t|)$. With $\boldsymbol{Q}_{\nabla f} = \mathrm{i}\boldsymbol{k}F_1/U_{\mathrm{e}}$ obtained from (25a) and (26) for specified values of parameters, the right-hand side of (29) can be computed numerically once $G_u(\boldsymbol{k},\omega)$ is specified. Following Hinze (1975), the two selections

$$g_{u,1}(r,\tau) = [1-\pi r^2/16]\,\mathrm{e}^{-\pi(r^2+\tau^2)/16}, \quad G_{u,1}(\boldsymbol{k},\omega) = (32/\pi^4)\, k^2\, \mathrm{e}^{-4(\mathrm{k}^2+\omega^2)/\pi} \tag{30}$$

and

$$g_{u,2}(r,\tau) = \mathrm{e}^{-(r^2+\tau^2)^{\frac{1}{2}}/2}\left[1-\frac{r^2}{4(r^2+\tau^2)^{\frac{1}{2}}}\right], \quad G_{u,2}(\boldsymbol{k},\omega) = \frac{64}{\pi^2}\frac{k^2}{[1+4(k^2+\omega^2)]^3} \tag{31}$$

were made, where $r\equiv|\boldsymbol{y}|$ and $\tau\equiv|t|$; $g_{u,1}$ characterizes flows with turbulence Reynolds numbers of order unity and $g_{u,2}$ is more appropriate for large turbulence Reynolds numbers (Hinze 1975).

In figure 2(a) we illustrate the quadratic dependence of the burning-velocity

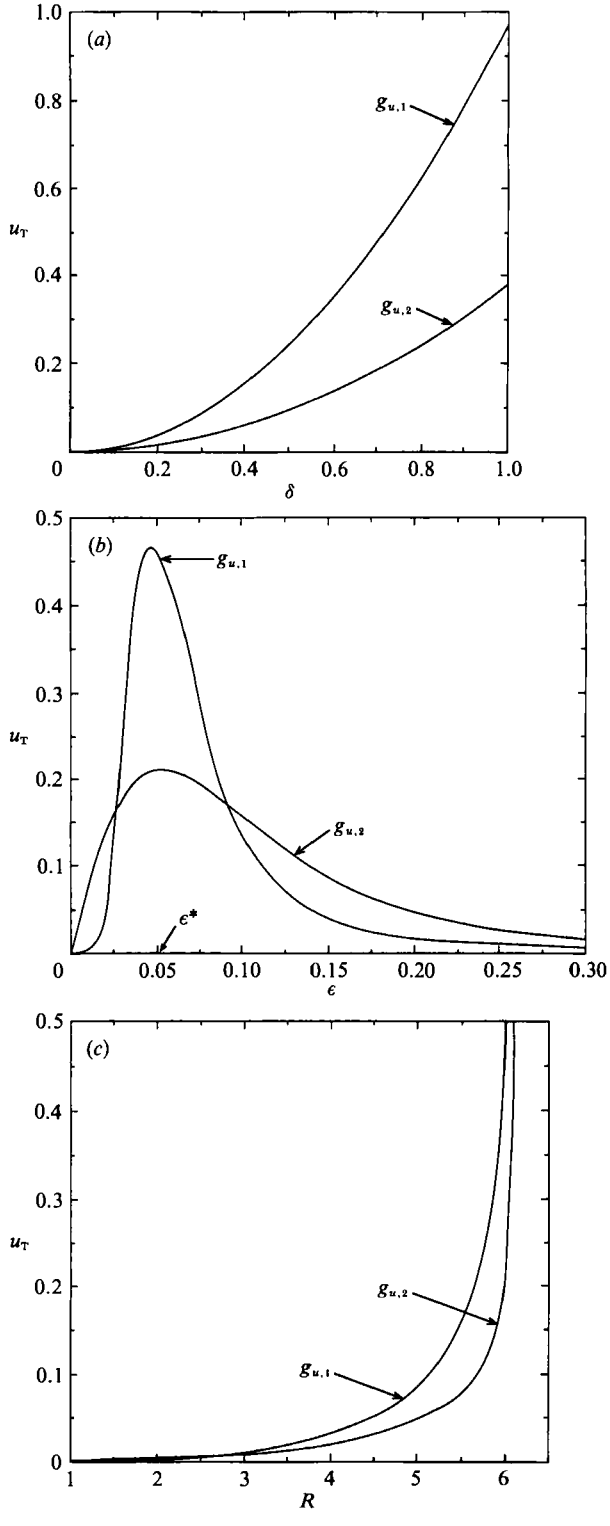

FIGURE 2. (*a*) The dependence of the fractional increment, u_T, in the turbulent burning velocity on (*a*) the relative turbulence intensity, δ, (*b*) the reciprocal, ϵ, of the non-dimensional turbulence scale, and (*c*) the unburnt-gas to burnt-gas density ratio, R. Each plot shows for two different forms, $g_{u,1}$ of (30) and $g_{u,2}$ of (31), for the autocorrelation function of the longitudinal component of the fluctuating turbulent velocity; stabilizing buoyancy factor $(R-1)\epsilon Ri = 1$ and $Pr = Le = 1$. (*a*) $R = 5$, $\epsilon = 0.05$; (*b*) $R = 5$, $\delta = 0.3$; (*c*) $\epsilon = 0.05$, $\delta = 0.3$.

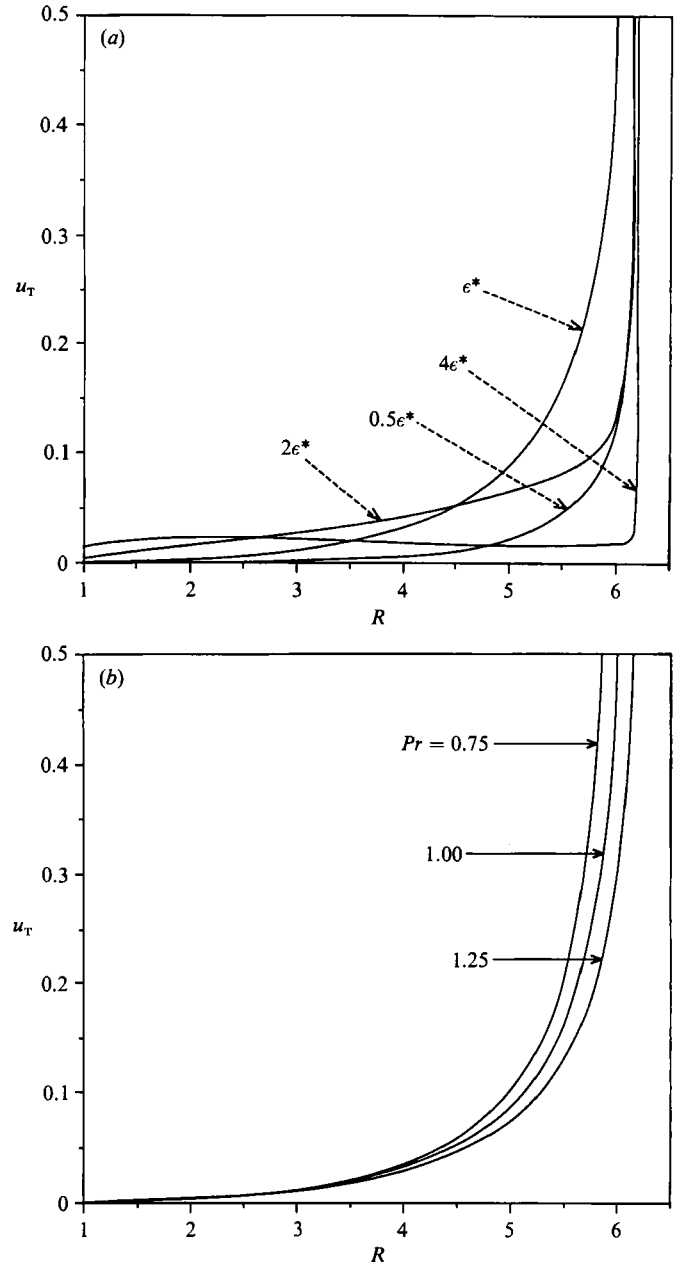

FIGURE 3(a, b). For caption see facing page.

increment on the turbulence intensity, implied by (27) and (29), by plotting u_T versus δ, taking $\epsilon = 0.05$, $R = Ri = 5$, $Pr = 1$, $s = [1+(R-1)\theta]^{\frac{1}{2}}$ and $\beta(Le-1) = 0$. This form for s, corresponding to the viscosity varying as the square root of the temperature, is qualitatively representative of gases and is adopted throughout. For the selected value of ϵ, the turbulent excitation field characterized by $g_{u,1}$ is seen to give larger values of u_T than that of $g_{u,2}$. This is a consequence of $G_{u,1}(\boldsymbol{k}, \omega)$ being larger than $G_{u,2}(\boldsymbol{k}, \omega)$ at the non-zero value of k at which $D(\boldsymbol{k}, \omega)$ in (26) has a minimum and of the fact that this value of k is of order unity when $\epsilon = \epsilon^* \equiv 0.05$.

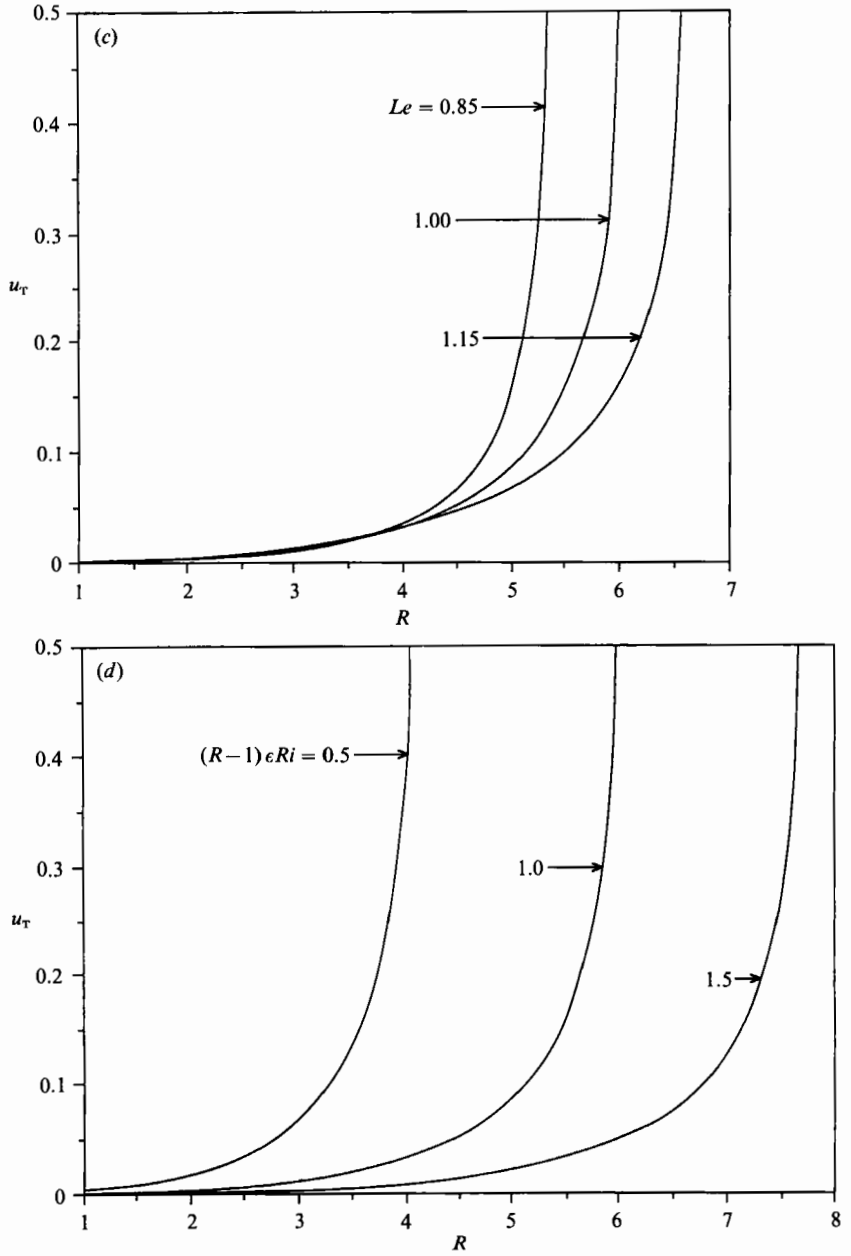

FIGURE 3. The dependence of the fractional increment, u_T, in the turbulent burning velocity on the density ratio R for various values of (*a*) the non-dimensional turbulence scale, $1/\epsilon$, (*b*) the Prandtl number Pr, (*c*) the Lewis number Le, and (*d*) the stabilizing buoyancy factor $(R-1)\epsilon Ri$; for $\delta = 0.3$. (*a*) $(R-1)\epsilon Ri = 1$, $Pr = Le = 1$; (*b*) $\epsilon = 0.05$, $(R-1)\epsilon Ri = 1$, $Le = 1$; (*c*) $(R-1)\epsilon Ri = 1$ and the Zel'dovich number $\beta = 10$; (*d*) $\epsilon = 0.05$, $Pr = Le = 1$.

Thus in this case $g_{u,1}$ selectively excites mainly the least-stable wavenumbers. In figure 2(*b*), however, where to show the effect of turbulence scale at fixed intensity we vary ϵ at $R = 6$, $Pr = 1$, $\beta(Le-1) = 0$, $\delta = 0.3$ and the Richardson number based on the flame thickness $\epsilon Ri = 0.25$, we see that $g_{u,2}$ gives slightly larger values of u_T when ϵ is sufficiently far from the neighbourhood of ϵ^*, mainly because the peak of

$G_{u,1}$ in the vicinity of $k = 1$ is narrower than that of $G_{u,2}$. This figure demonstrates that u_T is large when the turbulence scales coincide with the least-stable wavelength, the minimum of $D(\boldsymbol{k}, \omega)$, and smaller for both larger and smaller turbulence scales. Figure 2(*c*) shows the increase in u_T with increasing density ratio R, associated with the decrease in the damping at the least-stable wavenumber with increasing R, present in (26). The great difference in values of u_T between use of $g_{u,1}$ and $g_{u,2}$ obtained here near the planar-flame stability limit $R \approx 6$, where the flame becomes extremely sensitive to disturbances, is due again to the larger energy content of $g_{u,1}$ in the vicinity of the least-stable wavelength. For smaller values of R, however, the difference becomes negligible; here we have fixed $(R-1)\epsilon Ri = 1$ in varying R to maintain the stabilizing effect of gravity in the limit $R \to 1$.

In the remaining figures only $g_{u,1}$ of (30) is used to characterize the excitation field because the results from the two correlation functions are qualitatively similar (for brevity the subscript, 1 henceforth is omitted). Furthermore, because of the simple quadratic dependences of the averages on the relative intensity δ, all curves are shown only for the one value $\delta = 0.3$. Because of the strong influence of the density ratio R seen in figure 2(*c*), the remaining burning-velocity curves (figure 3) all show the fractional increment u_T as a function of R. The effect of the scale of turbulence, inversely proportional to ϵ at a fixed flame thickness, is shown in figure 3(*a*). The dependence of u_T on R is seen here to be very weak (except near the stability limit) for large and small ratios of ϵ/ϵ^* and is greatest for $\epsilon = \epsilon^*$, the value (0.05) for peak response defined in the previous paragraph. Figure 3(*b–d*) shows that smaller values of the parameters Pr, Le and Ri generally give higher values of u_T for a given value of R and a decreased stability limit. The effect of the Prandtl number, which enters through H in (26), as seen from (10*c*), is quite small but shows that increasing the viscosity with all else held fixed increases stability, as would be expected intuitively. The effect of the Lewis number, which enters through the Markstein length in (10*b*), is larger and is consistent with the known (Williams 1985) approach to the boundary of cellular instability with decreasing Le. The observed large effect of the Richardson number in figure 3(*d*) is also expected because of the reduction in stability with decreasing buoyancy.

Figure 4 shows $f' \equiv (\overline{f_1^2})^{\frac{1}{2}}$, a measure of the turbulent-flame-brush thickness (the extent of flame fluctuation about $\bar{x} = 0$) in units of the integral scale. Here we have fixed $\epsilon = 0.05$, $(R-1)\epsilon Ri = 1$ and $Pr = Le = 1$. Also plotted in this figure are the root-mean squares of the longitudinal velocity fluctuation at the flame front and the flame fluctuation speed, $u'_-(= u'_+)$ and $(\partial f/\partial t)'$ respectively, calculated at the lowest order in δ. In contrast to u_T, all quantities in figure 4 are proportional to intensity δ, instead of δ^2. We see that f' and u'_- increase in similar manners with increasing R and become very large near the stability limit. However, this is not true for $(\partial f/\partial t)'$, which does not follow the behaviour of u'_-, contrary to the prediction of the form of the flame-front evolution equation given in (16*d*) at the lowest order in ϵ. This occurs because gravity and diffusive–thermal effects, which arise through the term of order ϵ on the right-hand side of (16*d*), cancel the divergence that tends to develop in u'_- with increasing R, thereby reducing the speed of the flame relative to the flow. The cancellation is a consequence of the time derivative because from (26) it can be shown that the gas velocity and hence the flame displacement only diverge at zero frequency. This difference between u'_- and $(\partial f/\partial t)'$ has been seen in experiments cited previously (Clavin & Williams 1982), and the present results show it to be a consequence of the relatively large value of the density ratio R in typical real flames.

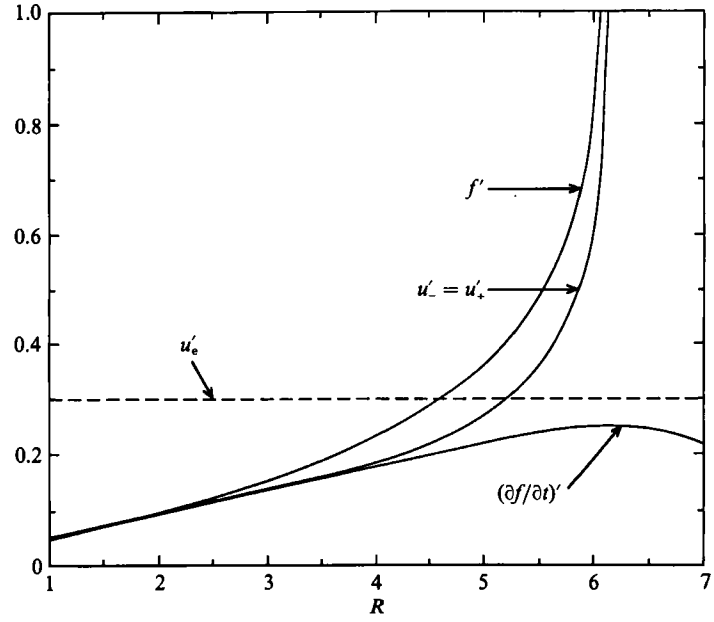

FIGURE 4. The dependence of the root-mean squares of the longitudinal velocity fluctuation in the laboratory frame, of the flame displacement and of the flame velocity on the density ratio R for $\delta = 0.3$, $\epsilon = 0.05$, $(R-1)\epsilon Ri = 1$ and $Pr = Le = 1$.

6. Turbulence-energy calculations

An influence of premixed flames on turbulent flows is the damping or amplification of turbulent kinetic energy across the flame and in the upstream and downstream hydrodynamic regions of the flow by the feedback of the flame-front dynamics on the upstream turbulence (Pelce & Clavin 1982; Searby & Clavin 1986; Clavin 1985). Here we define $q(x)$ as the total turbulence kinetic energy at the lowest order in δ, which has the longitudinal contribution $q_u(x)$ and the total transverse contribution $q_v(x)$; $q = q_u + q_v$. Through a procedure that is entirely analogous to that by which (29) is derived, it is found that

$$q_u(x) \equiv \tfrac{1}{2}\overline{u_1^2} = \tfrac{1}{2}\delta^2 \int_{-\infty}^{\infty} \mathrm{d}\boldsymbol{k} \int_{-\infty}^{\infty} \mathrm{d}\omega\, |U_1/U_e|^2 G_u(\boldsymbol{k},\omega). \tag{32}$$

To get a corresponding expression for q_v, we first write, using (23), (24) and (25e),

$$|V_1(k,\omega,x)|^2 = C_u(k,\omega,x)\,|U_e(k,\omega)|^2 + C_v(k,\omega,x)\,|V_e(k,\omega)|^2, \tag{33a}$$

$$C_u(k,\omega,x) = |A'(k,\omega,x)|^2 + 2\{[\mathrm{i}\omega + \epsilon Pr(\omega^2+k^2)]B'(k,\omega,x)\}\cdot A'(k,\omega,x)/k, \tag{33b}$$

$$\left.\begin{aligned} A'(k,\omega,x) &= (kP_-/U_e)\,\mathrm{e}^{kx}/(k+\mathrm{i}\omega) \\ B'(k,\omega,x) &= \mathrm{e}^{-[\mathrm{i}\omega+\epsilon Pr(\omega^2+k^2)]x} \end{aligned}\right\}, \quad x<0.$$

$$\left.\begin{aligned} A'(k,\omega,x) &= (kP_+/U_e)\,\mathrm{e}^{-kx}/(k-\mathrm{i}\omega/R) + kA\,\mathrm{e}^{-\{\mathrm{i}\omega/R+\epsilon Pr\,S[(\omega/R)^2+k^2]\}x} \\ B'(k,\omega,x) &= -B\,\mathrm{e}^{-\{\mathrm{i}\omega/R+\epsilon Pr\,S[(\omega/R)^2+k^2]\}x} \end{aligned}\right\}, \quad x>0,$$

$$C_v(k,\omega,x) = \mathrm{e}^{-2\epsilon Pr(\omega^2+k^2)x}, \quad x<0; \qquad C_v(k,\omega,x) = \mathrm{e}^{-2\epsilon Pr\,S[(\omega/R)^2+k^2]x}, \quad x>0, \tag{33c}$$

where the symbol $\cdot$ in (33b) denotes the inner product of two vectors in complex space. It can then be shown, for example by considering the right-hand side of (33a)

as representing the sum of contributions associated with purely longitudinal and purely transverse fluctuations, that

$$q_v(x) \equiv \tfrac{1}{2}\overline{|\boldsymbol{v}_1|^2} = \tfrac{1}{2}\delta^2 \int_{-\infty}^{\infty} \mathrm{d}\boldsymbol{k} \int_{-\infty}^{\infty} \mathrm{d}\omega [C_u(k,\omega,x)\, G_u(\boldsymbol{k},\omega) + C_v(k,\omega,x)\, G_v(\boldsymbol{k},\omega)] \quad (34)$$

for a turbulent excitation field which is isotropic, where G_u and G_v are Fourier transforms of the correlation functions for longitudinal and transverse exciter fluctuations, namely g_u given in (28) and

$$g_v(|y_2-y_1|, |t_2-t_1|) = \overline{\boldsymbol{v}_e(y_1,t_1)\cdot \boldsymbol{v}_e(y_2,t_2)}/\delta^2 \quad (35)$$

respectively.

Using (25) and (32)–(34), we can plot q, q_u and $\frac{1}{2}q_v$ (representative of the energy associated with one of the transverse components of velocity fluctuation) versus x, taking $G_u(\boldsymbol{k},\omega)$ as defined in (30) and

$$G_v(\boldsymbol{k},\omega) = (32/\pi^4)\,(k^2+2\omega^2)\,\mathrm{e}^{-4(k^2+\omega^2)/\pi}, \quad (36)$$

which is the spectrum for the transverse fluctuations in the fully isotropic turbulence corresponding to $g_{u,1}$ (Hinze 1975); (36) is the only choice for G_v consistent with the assumption of an isotropic excitation field with this $G_u(\boldsymbol{k},\omega)$. In the plots, which are shown in figures 5–7, the kinetic energies are normalized by the total excitation energy,

$$q_e(x) \equiv \tfrac{3}{2}\delta^2 \int_{-\infty}^{\infty} \mathrm{d}\boldsymbol{k} \int_{-\infty}^{\infty} \mathrm{d}\omega\, |U_1/U_e|^2 G_u(\boldsymbol{k},\omega), \quad (37)$$

where U_1 is given by (22), and the notations *total* $\equiv q(x)/q_e(x)$, *longitudinal* $\equiv q_u(x)/q_e(x)$, *transverse* $\equiv q_v(x)/2q_e(x)$ and *excitation* $\equiv q_e(x)$ are employed. Sufficiently far upstream where flame-induced effects on the flow are negligible, *total* = 1 and *longitudinal* = *transverse* = $\frac{1}{3}$. This state is represented by the horizontal dashed lines in the figures. Turbulent kinetic energy decays through viscous effects on the scale x/ϵ, and this is shown in the curve labelled *excitation* in figure 5, where we have taken $\epsilon = \epsilon^*$, $\delta = 0.3$, $R = 1$ and $Pr = Le = (R-1)\,\epsilon Ri = 1$. None of the other curves depend on the value of δ.

In figure 5 the gas-expansion effects on the jump conditions across the flame have been removed by putting $R = 1$, but the gravitational effects have been retained by keeping $(R-1)\,\epsilon Ri$ non-zero. When this is done, the extent of the hydrodynamic adjustment region is symmetric about $x = 0$; it is found to extend over about three integral lengthscales on each side of the flame, as may be seen in figure 5. The extent of flame fluctuation about $\bar{x} = 0$ is much smaller, however; $f' \approx 0.05$ at $\delta = 0.3$ for $R = 1$, according to figure 4. The non-monotonic modification of kinetic energies through the upstream and downstream hydrodynamic zones, in this case, is due to the coupling of gravity-induced oscillations with the longitudinal excitation field. This is shown clearly in (33), where neglecting the slow viscous decay we see that modification of q_v with increasing x is a result of competition between the growth or attenuation of the two terms on the right-hand side of (33*b*). The first term, associated directly with gravitational effects (see (25) for $R = 1$), monotonically increases (decreases) with increasing x in the region $x < 0$ ($x > 0$), while the second term, associated with the coupling between gravitational oscillations and the excitation field, may increase *or* decrease depending on the phase of the excitation function $B'(k,\omega,x)$, which varies linearly with x.

Physically, gravity-induced amplification occurs when gravity-induced oscillations

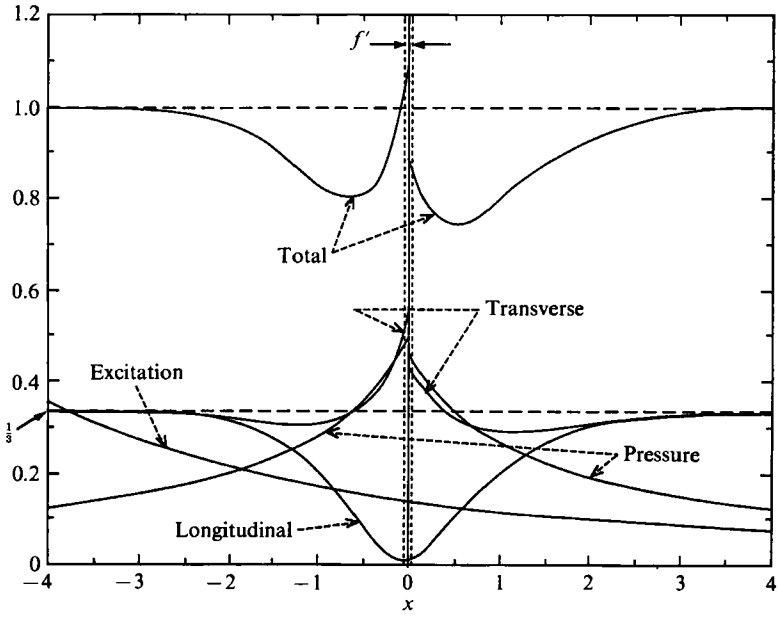

FIGURE 5. The evolution of the relative turbulent kinetic energies and (for $\delta = 0.3$) pressure through the hydrodynamic zones for $\epsilon = 0.05$, $R = 1$, $(R-1)\epsilon Ri = 1$ and $Pr = Le = 1$.

are in phase with excitation fluctuations over a significant portion of the wavenumber and frequency spectrum, and the extent of this resonance varies with x. Since the effect of gravity is to resist motion of the flame about $x = 0$ and at the lowest order $\partial f_1/\partial t = u_{1-} = u_{1+}$, longitudinal velocity fluctuations are smallest at the flame front. By mass conservation the effects of gravity on longitudinal and transverse fluctuations are opposite, so that q_v tends to be largest near the flame, as seen in figure 5. The discontinuous decrease in q_v across the flame for values of R near unity, seen in figure 5, is the opposite of the well-known (Clavin & Williams 1982) effect of gas expansion on the transverse velocity fluctuations. The cause of this discontinuity can be seen by neglecting the highest-order viscous terms in (16*b*) to observe that for $R = 1$ the damping of $v_1(y, t)$ across the flame is due primarily to the conservation of tangential momentum and resulting streamline deflection, when the flame is tilted, associated with a difference in gravitational potential across the flame. Since (16*b*) gives at the lowest order $\overline{|v_{1+}|^2} - \overline{|v_{1-}|^2} = 2J[(R-1)\epsilon Ri]\,\overline{v_{1-}\cdot\nabla f_1}$, the decrease in q_v across the flame is a consequence of v_{1-} being out of phase with ∇f_1 on the average through the effect of gravity on transverse fluctuations discussed above. The decrease in *total* across the flame shown in figure 5 is a result only of the decrease in *transverse* since there is no change in u_1 across the flame in this case (see (16*a*)).

Although these gravity effects are enhanced with gas expansion, there is an additional, destabilizing effect for $R > 1$ resulting from the hydrodynamic instability associated with streamline deflection in the hydrodynamic zones (Williams 1985; Clavin 1985). In figure 6(*a*) we take $R = 4$ with the same values for the other parameters as in figure 5 and find that the extent of flame-induced damping or amplification of q_u and q_v upstream of the flame is reduced, while the extent of modification in the downstream adjustment zone is increased. Across the flame q_v is strongly amplified, primarily because the tendency toward hydrodynamic instability produced by the second term on the right-hand side of (16*b*) dominates the damping

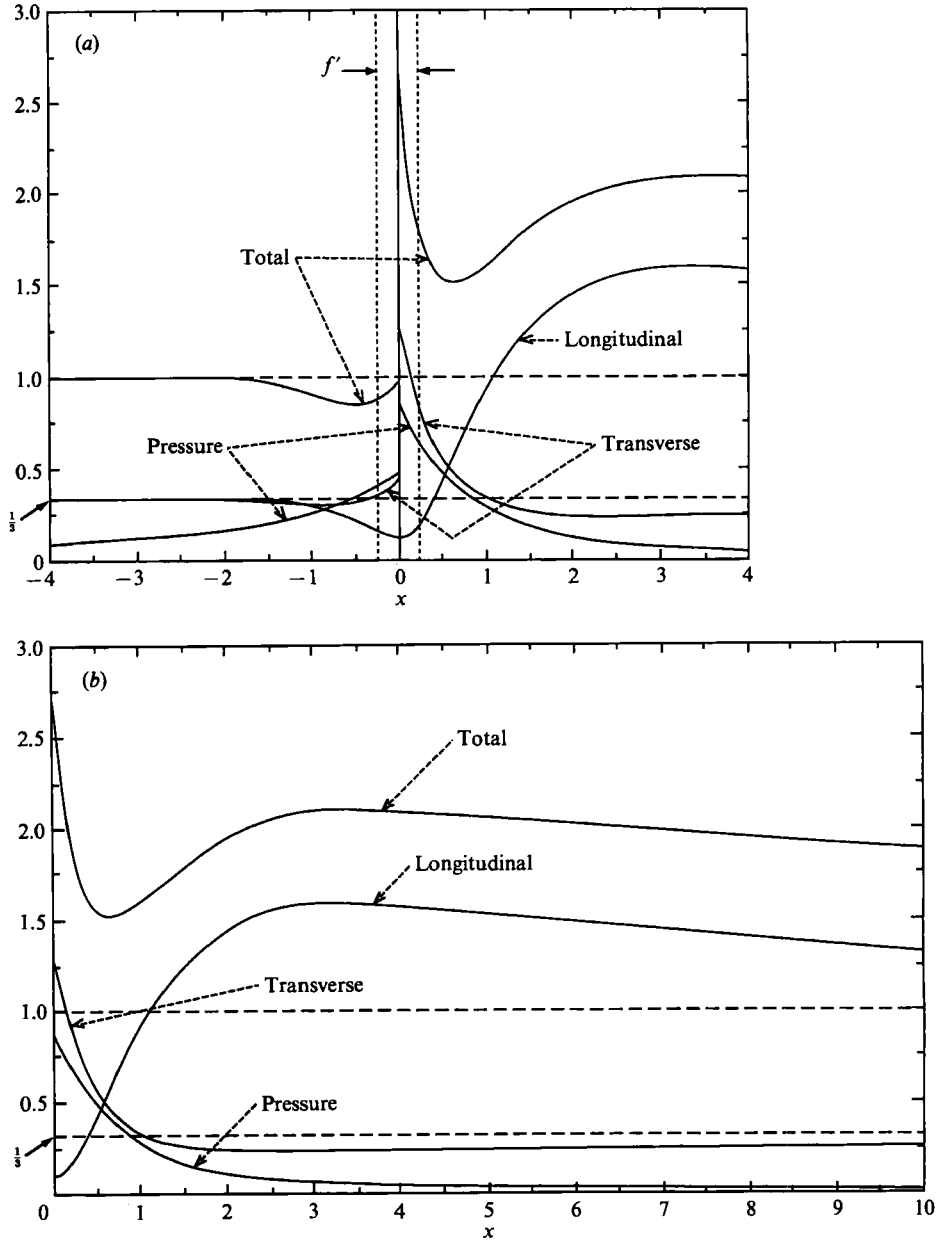

FIGURE 6. The evolution of the relative turbulent kinetic energies and (for $\delta = 0.3$) pressure through (*a*) the hydrodynamic zones and (*b*) the downstream hydrodynamic zone, for $\epsilon = 0.05$, $R = 4$, $(R-1)\epsilon Ri = 1$ and $Pr = Le = 1$.

effect of gravity produced by the term involving $Ri\nabla f_1$. Within the downstream hydrodynamic adjustment zone there is a rapid transfer of turbulent kinetic energy from transverse to longitudinal fluctuations and an associated dip in the total kinetic energy. Slow decay of the relative longitudinal energy occurs because q_u has a faster viscous decay rate than that of q_e for this selection of parameters (see figure 6*b*). The value of f' is approximately 0.25 at $\delta = 0.3$ for this case, according to figure 4; the pressure profiles will be discussed later.

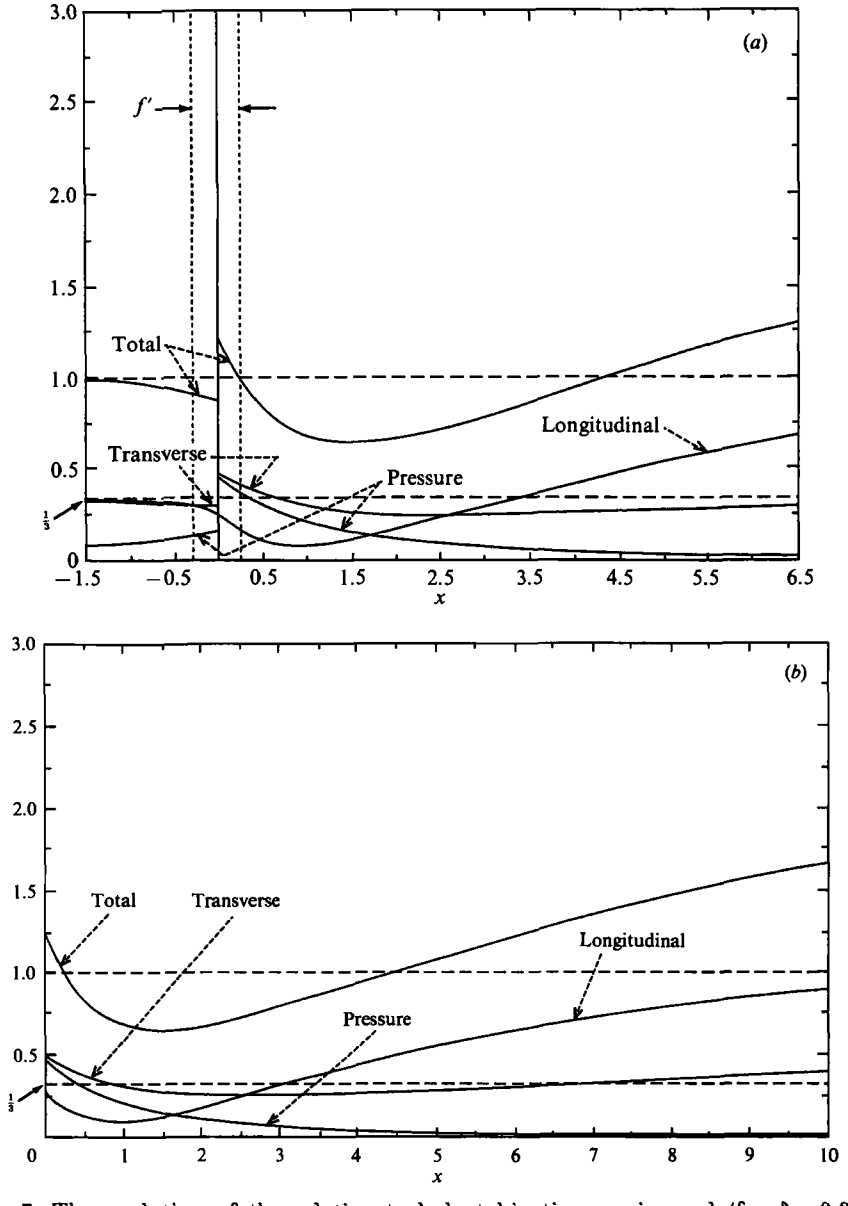

FIGURE 7. The evolution of the relative turbulent kinetic energies and (for $\delta = 0.3$) pressure through (*a*) the hydrodynamic zones and (*b*) the downstream hydrodynamic zone for $\epsilon = 0.2$, $R = 4$, $(R-1)\epsilon Ri = 1$ and $Pr = Le = 1$.

In figure 7 (*a*) we take $\epsilon = 4\epsilon^*$ and the same values for the other parameters as in figure 6 in order to investigate the effect of smaller turbulence lengthscales. Here we see that the extent of flame-induced modification of q_u and q_v in the upstream and downstream hydrodynamic adjustment zones and in the jump of q_v across the flame is reduced in comparison with figure 6 because of the stabilizing diffusive–thermal effect (Williams 1985) which is larger than the effects of gravity and hydrodynamic instability at large wavenumbers. Beyond the downstream adjustment zone the normalized energies continue to increase with x because q_u and q_v have slower viscous

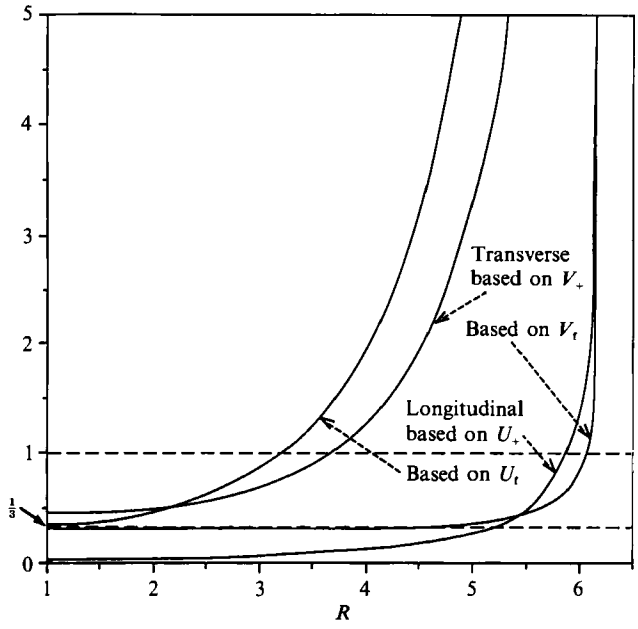

FIGURE 8. The dependences of the relative fluctuation intensities of longitudinal and transverse velocity components on the density ratio R, just downstream from the flame and in the final flow, for $\epsilon = 0.05$, $(R-1)\epsilon Ri = 1$ and $Pr = Le = 1$.

decay rates than that of q_e for this selection of parameters (see figure 7*b*), the turbulence scales induced by the flame having been predominantly larger than those of the excitation field.

In figure 5 it is seen that with $R = 1$ the initially isotropic turbulence eventually returns to isotropy after passing through the flame. However, figures 6 and 7 show that the anisotropy produced by the flame continues to persist when gas expansion is present. Although the jumps across the flame generate this anisotropy in transverse fluctuations, the adjustments in the downstream hydrodynamic zone transfer the intensity to longitudinal fluctuations, so that the final anisotropy (far downstream from the flame) exhibits higher longitudinal intensities than transverse intensities when $R > 1$. The reason for this final anisotropy in velocity fluctuations beyond the downstream adjustment zone is the production of vorticity by the flame in transverse directions, which results in larger vorticity intensities in transverse directions than in the longitudinal direction (refer to §7). The generation of fluctuations of velocity and vorticity by the flame in transverse directions results in a shorter characteristic lengthscale for longitudinal fluctuations than that for transverse fluctuations. However, the existence of pressure–strain correlations and the fact that the flame-generated vorticity is conserved through the downstream region results in a changing characteristic lengthscale for longitudinal fluctuations causing it to become longer than that for transverse fluctuations far downstream from the flame. In figure 8 we investigate the effect of the magnitude of R on the final anisotropy. Taking the same values for the other parameters as in figure 6, we plot the longitudinal and transverse components of the normalized turbulence energy, which are based on U_+ and V_+ respectively at the downstream side of the flame and on U_f and V_f respectively far downstream from the flame when viscous decay is neglected (see (24*c*) and (24*e*)). As R is increased we observe that the energy

associated with transverse fluctuations based on V_f remains nearly constant, except near the stability limit, while the longitudinal component of energy based on U_f increases rapidly. Therefore, the final total turbulent kinetic energy (with viscous decay removed) and extent of anisotropy in longitudinal fluctuations both increase with increasing R. We have found this effect of gas expansion to be qualitatively independent of the parameters Pr, Le, Ri and ϵ, and it may therefore be considered to be of general validity in the limit of large-scale turbulence.

Although earlier studies have not addressed the variations of turbulent kinetic energies in the hydrodynamic zones, shown in figures 5–7, consideration has been given to the jump in turbulent kinetic energy across the flame with body–force and diffusive–thermal effects neglected (Clavin & Williams 1982). It was pointed out in Clavin & Williams (1982) that the flame-tilt effect, which is central to the hydrodynamic instability, enhances the turbulent kinetic energy in transverse components to such an extent that the total turbulent kinetic energy of the fluid per unit mass, and even per unit volume, increases when the fluid crosses the flame if R is sufficiently large. However, because of a sign error in the application of a Taylor hypothesis, (40) and (41) of Clavin & Williams (1982), giving expressions for these changes, are incorrect in their second-order terms accounting for finite R. There are corresponding errors in subsequent results quoted in that paper for relative turbulence intensities in transverse fluctuation; in particular, in the present notation, for turbulence that is isotropic just upstream from the flame the ratio of a transverse component of intensity to the longitudinal component is $[1+(R-1)(R-2)]^{\frac{1}{2}}$, rather than $[1+R(R-1)]^{\frac{1}{2}}$, which now achieves a minimum at $R=\frac{3}{2}$ instead of increasing monotonically with R for $R>1$. An important result of the present analysis is that the anisotropy at large R, exhibiting a large ratio of transverse to longitudinal intensities just downstream from the flame, is transformed into a large ratio of longitudinal to transverse intensities farther downstream as the flow traverses the downstream hydrodynamic zone.

In addition to turbulence energies, the calculation of pressure fluctuations is of interest. It may be shown that at the lowest order in δ the pressure field that would be measured in the laboratory reference frame is given by the Fourier inverse of $P_- e^{kx}$ for $x<0$ and of $P_+ e^{-kx}$ for $x>0$. The root-mean-square pressure fluctuations measurable in the laboratory frame are therefore given by $p' \equiv [\overline{(p_1+Rif_1)^2}]^{\frac{1}{2}}$, $x<0$, and $p' \equiv [\overline{(p_1+Rif_1/R)^2}]^{\frac{1}{2}}$, $x>0$ (see (24a)), and their variations through the hydrodynamic flow field are shown in figures 5–7. We observe that the flame induces pressure fluctuations which are maximum near the flame, decreasing to zero in either direction away from $x=0$. In crossing the flame the flow experiences an increase in its pressure fluctuation, like its transverse velocity fluctuations, when R is not small (see figure 6a). In figure 9 we plot p' and the root-mean-squares of the longitudinal and transverse velocity fluctuations at the flame, as well as the root-mean square pressure fluctuation in the moving coordinate system at the leasing order in ϵ denoted as $p_1' \equiv (\overline{p_1^2})^{\frac{1}{2}}$, as functions of R. The divergence of the latter as $R \to 1$ is a low-frequency gravity-wave effect, as may be seen from (24a) and (26); otherwise this curve tends to follow that of p_+'. Values of all quantities on the upstream side of the flame are seen to be affected very little by increasing R for stable flames, while on the downstream side pressure and transverse velocity fluctuations increase strongly with increasing R, the longitudinal velocity fluctuations being much less sensitive. The vorticity curve in figure 9 is discussed in the following section.

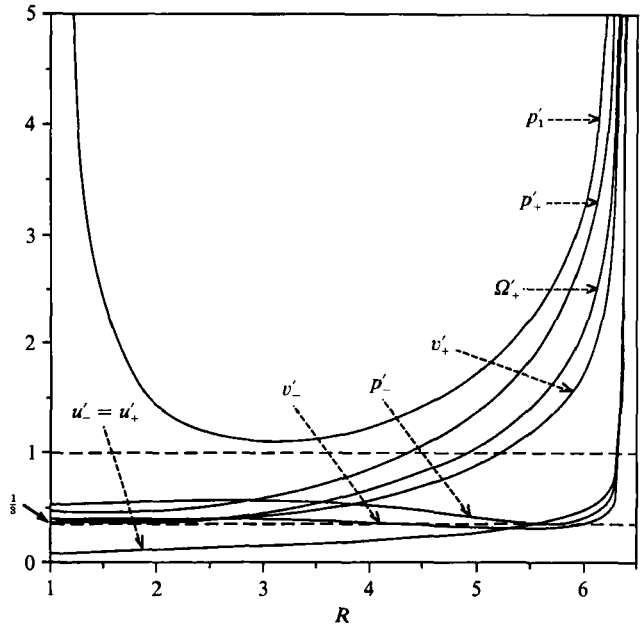

FIGURE 9. The dependences of the root-mean square pressure, velocity and vorticity fluctuations at the flame on the density ratio R for $\delta = 0.3$, $\epsilon = 0.05$, $(R-1)\epsilon Ri = 1$ and $Pr = Le = 1$.

7. Turbulence–vorticity generation

Turbulence in the hydrodynamic regions in general will have components of vorticity Ω_x and Ω_y in the longitudinal and transverse directions, respectively. Cartesian vorticity components are

$$\left.\begin{aligned} \Omega_x &\equiv \partial w/\partial y - \partial v/\partial z, \\ \Omega_y &\equiv \partial u/\partial z - \partial w/\partial x, \\ \Omega_z &\equiv \partial v/\partial x - \partial u/\partial y, \end{aligned}\right\} \tag{38}$$

where v and w are the components of the velocity vector $\boldsymbol{v}$ in the transverse directions y and z, respectively, and Ω_y and Ω_z are, similarly, components of the transverse vorticity vector $\boldsymbol{\Omega}_y$. The root-mean-square vorticity fluctuations Ω_x', Ω_y' and Ω_z' are obtained from knowledge of the Fourier transforms of Ω_x and Ω_y, denoted as Ω_ω and Ω_k, respectively. Similar to the above calculations of turbulent flame speed and turbulent kinetic energies (for example, see (29)), the square magnitudes of these transforms are used to give ensemble-average square vorticity fluctuations.

Taking the Fourier transform of (38) and then using (24*b*) and (24*d*), we find for the flow upstream of the flame that

$$\left.\begin{aligned} \Omega_\omega &= (\mathrm{i}k_y W_\mathrm{e} - \mathrm{i}k_z V_\mathrm{e})\, C_\mathrm{e}(x), \\ \Omega_{k_y} &= \mathrm{i}k_z C_\mathrm{e}(x)\, U_\mathrm{e} - [\partial C_\mathrm{e}(x)/\partial x]\, W_\mathrm{e}, \\ \Omega_{k_z} &= -\{\mathrm{i}k_y C_\mathrm{e}(x)\, U_\mathrm{e} - [\partial C_\mathrm{e}(x)/\partial x]\, V_\mathrm{e}\}, \end{aligned}\right\} \quad x < 0, \tag{39}$$

where $C_\mathrm{e}(x) = \mathrm{e}^{-[1\omega + \epsilon Pr(\omega^2+k^2)]x}$, k_y and k_z are the components of the wave-number vector $\boldsymbol{k}$, and V_e and W_e are the components of the transverse excitation-field vector

V_e. Equation (39) reveals upon comparison with (22) that there is no flame-induced modification of vorticity upstream from the flame; the upstream vorticity field everywhere equals the excitation vorticity field, as it must according to the equation for vorticity transport. For the downstream hydrodynamic region, using (24*c*), (24*e*) and (25*e*), we find

$$\left.\begin{aligned} \Omega_\omega &= (\mathrm{i}k_y W_e - \mathrm{i}k_z V_e)\, C_f(x), \\ \Omega_{k_y} &= \mathrm{i}k_z C_f(x)\, U_f - [\partial C_f(x)/\partial x]\, W_f, \\ \Omega_{k_z} &= -\{\mathrm{i}k_y C_f(x)\, U_f - [\partial C_f(x)/\partial x]\, V_f\}, \end{aligned}\right\} \quad x > 0, \tag{40}$$

where $C_f(x) = \mathrm{e}^{-\{1\omega/R + \epsilon Pr\, S[(\omega/R)^2 + k^2]\}x}$. Equation (40) shows that there is of course no generation of vorticity in the downstream hydrodynamic zone (since the square magnitudes of these transforms vary only on the long viscous-decay scale x/ϵ). Vorticity may, however, be produced or consumed across the flame as a result of the baroclinic coupling between density and pressure gradients that occurs in the flame and is attributed to the cross-product of $\bar{\nabla}u_0$ and $\bar{\nabla}p$ in the vorticity equation, the overbar indicating laboratory coordinates $(\bar{x}, \bar{y}, \bar{z})$. Since at the lowest order in δ density gradients in transverse directions are zero, the components of this cross-product in the longitudinal direction is zero, and it is found (compare the first relations of (39) and (40)) that no modification of the longitudinal component of vorticity across the flame occurs at this order. The rates of viscous decay downstream from the flame are different from those upstream, however, when $R \neq 1$ or $S \neq 1$, as may be seen by comparing $C_e(x)$ with $C_f(x)$. The components Ω'_y and Ω'_z will generally be modified across the flame and are the subject of the following investigation.

Since the vorticity field upstream is equal to the excitation vorticity field which we assume to be isotropic, $\Omega'_x = \Omega'_y = \Omega'_z$ for $x < 0$, either Ω'_y or Ω'_z may be used to characterize the intensity of vorticity in this region. Taking the square magnitudes of Ω_{k_y} and Ω_{k_z} given in (39) we find, using (22) and (23),

$$|\Omega_{k_y}|^2 + |\Omega_{k_z}|^2 = [(k^2 + 2\omega^2)\,|U_e|^2 + \omega^2\,|V_e|^2]\,|C_e(x)|^2, \quad x < 0. \tag{41}$$

Upstream of the flame the root-mean-square vorticity fluctuation in any direction Ω'_e is then given by

$$2[\Omega'_e(x)]^2 \equiv \overline{\Omega_y^2}(x) + \overline{\Omega_z^2}(x) = \delta^2 \int_{-\infty}^{\infty} \mathrm{d}\boldsymbol{k} \int_{-\infty}^{\infty} \mathrm{d}\omega\, [(k^2 + 2\omega^2)\, G_u(\boldsymbol{k}, \omega) + \omega^2 G_v(\boldsymbol{k}, \omega)]\, |C_e(x)|^2. \tag{42}$$

Taking $G_u(\boldsymbol{k}, \omega)$ from (30) and $G_v(\boldsymbol{k}, \omega)$ from (36), we then obtain

$$[\Omega'_e(x)]^2 = \frac{16}{\pi^4}\delta^2 \int_{-\infty}^{\infty} \mathrm{d}\boldsymbol{k} \int_{-\infty}^{\infty} \mathrm{d}\omega (k^4 + 3k^2\omega^2 + 2\omega^4)\, \mathrm{e}^{-4(k^2+\omega^2)\,(1+\epsilon\pi Pr\, x/2)/\pi}, \tag{43}$$

which may be evaluated analytically to give

$$\Omega'_e = \frac{(5\pi/8)^{\frac{1}{2}}\delta}{(1 + \frac{1}{2}\epsilon\pi\, Pr\, x)^{\frac{7}{4}}}. \tag{44}$$

For the downstream hydrodynamic zone, (40) gives

$$|\Omega_{k_y}|^2 + |\Omega_{k_z}|^2 = \{[k^2|U_f/U_e - C_+ A|^2 - 2(U_f/U_e - C_+ A)(C_- C_+ B)]\,|U_e|^2 + |C_+|^2\,|V_e|^2\}\,|C_f(x)|^2, \quad x > 0. \tag{45}$$

where A and B are defined in (25*e*) and C_- and C_+ denote $\partial C_e/\partial x$ and $\partial C_f/\partial x$,

respectively, each evaluated at $x = 0$. Integrating over (45) we obtain an expression for $\Omega' \equiv \Omega'_y = \Omega'_z$ for $x > 0$, namely

$$2[\Omega'(x)]^2 \equiv \overline{\Omega_y^2}(x) + \overline{\Omega_z^2}(x) = \delta^2 \int_{-\infty}^{\infty} \mathrm{d}\boldsymbol{k} \int_{-\infty}^{\infty} \mathrm{d}\omega \{[k^2 |U_\mathrm{f}/U_\mathrm{e} - C_+ A|^2 - 2(U_\mathrm{f}/U_\mathrm{e} - C_+ A) \cdot (C_- C_+ B)] G_u(\boldsymbol{k}, \omega) + |C_+|^2 G_v(\boldsymbol{k}, \omega)\} |C_\mathrm{f}(x)|^2. \quad (46)$$

Equation (46) enables the intensity of transverse components of vorticity fluctuation downstream to be calculated and compared with those upstream.

For the selection of parameters $\epsilon = 0.05$, $(R-1)(\epsilon R) = 1$, $Pr = Le = 1$ and $\delta = 0.3$ – and with the expressions for G_u and G_v used in (43) – the right-hand side of (46) was calculated numerically. In Figure 9 the root-mean-square transverse vorticity fluctuation at the downstream edge of the flame Ω'_+ is plotted versus R. The longitudinal component remains constant, independent of R, equal to the value of that for the excitation field at $x = 0$, $\Omega'_\mathrm{e} = 0.42$ according (44). Therefore the vorticity generation or reduction by the flame is expressed entirely in terms of Ω'_+, the representative behaviour of which appears in figure 9. It is found for these values of parameters that $\Omega'_+ < \Omega'_\mathrm{e}$ when $1 < R \lesssim 2.75$, that is, at the smaller density ratios the flame reduces the root-mean-square vorticity fluctuations slightly. However, in the range of practical density ratios, $R \gtrsim 2.75$, there is appreciable generation of vorticity fluctuation by the flame, and this generation of Ω'_+ increases strongly with increasing R, as do p'_+ and v'_+ in figure 9. This generation is associated with a correlation between a transverse vorticity component and the component of the transverse pressure gradient orthogonal to it; the vorticity gives rise to bulges of the flame sheet, and through Bernoulli's principle the pressure tends to be higher in upstream-pointing bulges than in downstream-pointing bulges, thereby effecting the correlation.

Figures 6(*b*) and 7(*b*), for example, have shown the interchange of longitudinal and transverse velocity fluctuations in the downstream hydrodynamic zone. The pressure effects that lead to this interchange are absent in the equation for vorticity transport, and therefore the vorticity generated in transverse components remains in transverse components and is not transferred to longitudinal components. In the downstream hydrodynamic zone all components of vorticity fluctuations simply decay at the rate associated with $C_\mathrm{f}(x)$. At realistic values of R, therefore, while the far-downstream velocity fluctuations are predominantly longitudinal for an incoming isotropic turbulence, those of vorticity are predominantly transverse.

8. Conclusion

We have presented an analysis of the feedback between a stable, wrinkled premixed flame and an incoming weakly turbulent flow under conditions of statistical stationarity and transverse homogeneity and for an arbitrary value of the gas-expansion ratio R. This analysis extends the work of Searby & Clavin (1986) to the calculation of flame-induced modifications of turbulence properties in the upstream and downstream hydrodynamic regions of the flow and to an investigation of the effects of gas expansion and turbulence lengthscale on these modifications.

Parametric dependences of turbulent burning velocities on turbulence intensity, turbulence lengthscales, gas expansion, gravitational strength, and Lewis and Prandtl numbers have been obtained, showing effects of these parameters that are comprehensible on physical grounds. The variations in components of turbulent

kinetic energies through upstream and downstream hydrodynamic zones and across the flame have been calculated, indicating substantial modifications in turbulent kinetic energy components through the hydrodynamic zones, often resulting in nearly complete transfer of fluctuating energy from transverse to longitudinal modes within the downstream hydrodynamic zone. Root-mean-square pressure fluctuations were shown to be maximum near the flame and at realistic density ratios to be larger in the burnt gas than in the fresh mixture, like the intensity of transverse velocity fluctuations at the flame. The vorticity field in the upstream hydrodynamic zone was shown to be uninfluenced by flame dynamics, that is, to be everywhere equal to the incoming vorticity field in this region, and the longitudinal component of vorticity was found to be unmodified across the flame, but the root-mean-square transverse vorticity fluctuation is significantly increased by the flame at realistic values of the gas expansion ratio. In addition to these main results, many other details of the influence of the flame on the turbulence were derived.

This analysis sets the basis for future studies of effects of nonlinearities in premixed turbulent flame propagation. It is expected that nonlinear corrections will reduce the rate of increase of the turbulent burning velocity with increasing turbulence intensity (see figure 2*a*), since this rate is known to be constant at large intensities (Aldredge 1990; Williams 1985). It is desirable to ascertain the effects of nonlinearities on the conservation of vorticity through the hydrodynamic adjustment zones, such as vortex stretching, which might alter the extent of energy transfer between components of velocity fluctuation downstream from the flame. Furthermore, by retaining weak nonlinearities in the analysis, weakly unstable flame propagation may be investigated for the practically interesting regime of order-unity gas expansion. Previous analyses of flame propagation in unstable regimes have all restricted attention to the case of small gas expansion.

Partial support for this research was provided by the National Science Foundation through Grant No. CTS-8918527. The first author wishes to thank AT&T Bell Laboratories for fellowship support during this research. We are indebted to Drs P. Clavin and F. Joulin for helpful discussions about this work.

REFERENCES

ALDREDGE, R. C. 1990 Theory of premixed flame propagation in large-scale turbulence. Ph.D. dissertation, Princeton University.

BATCHELOR, G. K. 1956 *The Theory of Homogeneous Turbulence*. Cambridge University Press.

CLAVIN, P. 1985 *Prog. Energy, Combust. Sci.* **11**, 1.

CLAVIN, P. & GARCIA-YBARRA, P. 1983 *J. Méch. Theor. Appl.* **2**, 245.

CLAVIN, P. & WILLIAMS, F. A. 1979 *J. Fluid Mech.* **90**, 589.

CLAVIN, P. & WILLIAMS, F. A. 1982 *J. Fluid Mech.* **116**, 251.

HINZE, J. O. 1975 *Turbulence*, 2nd edn. McGraw-Hill.

PELCE, P. & CLAVIN, P. 1982 *J. Fluid Mech.* **124**, 219.

SEARBY, G. & CLAVIN, P. 1986 *Combust. Sci. Technol.* **46**, 167.

WILLIAMS, F. A. 1985 *Combustion Theory*, 2nd edn. Addison-Wesley.